Cell Systems

Article

Diclofenac and acetaminophen dim the acute-phase response but amplify expression of the iron regulator hepcidin in liver cancer cells

Graphical abstract

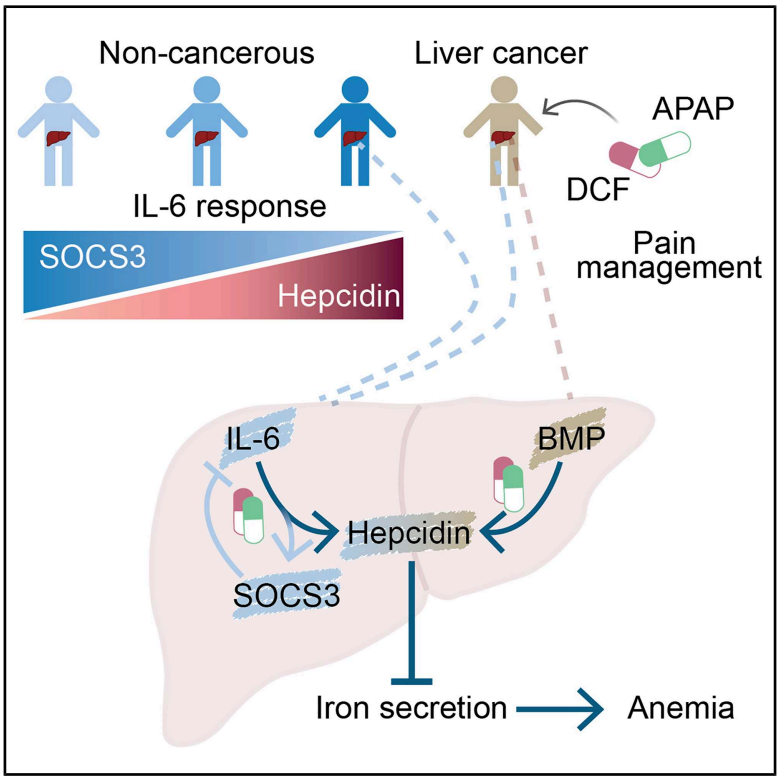

Authors

Anja Zeilfelder, Joep Vanlier, Christina Mölders, ..., Marcel Schilling, Jens Timmer, Ursula Klingmüller

Correspondence

jeti@fdm.uni-freiburg.de (J.T.), u.klingmueller@dkfz.de (U.K.)

In brief

In liver cells, non-opioid analgesic pain killers inhibit IL-6-induced acute-phase response but amplify hepcidin expression in hepatoma cells by autocrine BMP secretion, which can be inhibited by targeted intervention. In non-cancerous hepatocytes, the strength of the IL-6-induced negative feedback loop determines the patient-specific impact on hepcidin expression.

Highlights

- Acetaminophen (APAP) and diclofenac (DCF) alter IL-6 signaling via SOCS3 expression
- In HepG2 cells, DCF and APAP stabilize BMP-receptor interaction amplifying HAMP
- DCF and APAP's effects on SOCS3 and HAMP are patient specific
- Inhibition of BMP receptor with dorsomorphin blocks drug-induced HAMP expression

Zeilfelder et al., 2025, Cell Systems *16*, 101431
November 19, 2025
https://doi.org/10.1016/j.cels.2025.101431

CellPress

Cell Systems

CellPress
OPEN ACCESS

Article

Diclofenac and acetaminophen dim the acute-phase response but amplify expression of the iron regulator hepcidin in liver cancer cells

Anja Zeilfelder,[1,2,10] Joep Vanlier,[3,10] Christina Mölders,[1,2,10] Philipp Kastl,[1] Barbara Helm,[1] Sebastian Burbano de Lara,[1] Till Möcklinghoff,[1,2] Nantia Leonidou,[1] Elisa Holstein,[1,2] Artyom Vlasov,[1] Alexander Held,[1] Silvana Wilken,[1,4] Katrin Hoffmann,[4] Gerda Schicht,[5] Andrea Scheffschick,[5] Markella Katerinopoulou,[4] Esther Giehl-Brown,[4] Christoph Kahlert,[4] Christoph Michalski,[4] Daniel Seehofer,[5] Georg Damm,[5] Martina U. Muckenthaler,[6,7,8,9] Marcel Schilling,[1] Jens Timmer,[3,*] and Ursula Klingmüller[1,9,11,*]

[1]Division Systems Biology of Signal Transduction, German Cancer Research Center (DKFZ), 69120 Heidelberg, Germany
[2]Faculty of Biosciences, Ruprecht-Karls-University Heidelberg, 69120 Heidelberg, Germany
[3]Institute of Physics, University of Freiburg and Signalling Research Centres BIOSS and CIBSS, University of Freiburg, 79104 Freiburg, Germany
[4]Department of General, Visceral, and Transplantation Surgery, Heidelberg University Hospital, 69120 Heidelberg, Germany
[5]Department of Hepatobiliary Surgery and Visceral Transplantation, Clinic and Polyclinic for Visceral, Transplant, Thoracic and Vascular Surgery, Leipzig University Medical Center, 04103 Leipzig, Germany
[6]Department of Paediatric Hematology, Oncology and Immunology, University of Heidelberg, 69120 Heidelberg, Germany
[7]Molecular Medicine Partnership Unit, University of Heidelberg, 69120 Heidelberg, Germany
[8]German Centre for Cardiovascular Research (DZHK), Partner site Heidelberg/Mannheim, 69120 Heidelberg, Germany
[9]Translational Lung Research Center Heidelberg (TLRC), German Center for Lung Research (DZL), University of Heidelberg, 69120 Heidelberg, Germany
[10]These authors contributed equally
[11]Lead contact
*Correspondence: jeti@fdm.uni-freiburg.de (J.T.), u.klingmueller@dkfz.de (U.K.)
https://doi.org/10.1016/j.cels.2025.101431

SUMMARY

Cancer patients frequently suffer from anemia and cancer-related pain, which can be treated by non-opioid analgesics such as diclofenac (DCF) and acetaminophen (APAP) attenuating inflammatory responses. The pro-inflammatory cytokine interleukin (IL)-6 triggers the expression of acute-phase proteins, including the iron regulator hepcidin. Using proteomics and dynamic pathway modeling, we show that DCF and APAP directly impact IL-6 signaling by enhancing the induction of the feedback-inhibitor suppressor of cytokine signaling 3 (SOCS3), reducing signal transducer and activator of transcription (STAT)3 phosphorylation, and decreasing the expression of most acute-phase proteins except for hepcidin. In primary human hepatocytes (PHHs), the impact depends on the patient-specific extent of SOCS3 induction, which is anti-correlated with hepcidin expression. Whereas, in liver cancer cells, DCF and APAP stabilize the interaction of autocrine secreted bone morphogenic protein (BMP) with its receptor, resulting in strongly amplified hepcidin expression. Our studies suggest that co-inhibition of the BMP receptor counteracts excessive hepcidin production upon treatment with pain-relieving drugs and could prevent iron-deficiency-caused anemia in liver cancer. A record of this paper's transparent peer review process is included in the supplemental information.

INTRODUCTION

During the progression of cancer, patients frequently experience increasing pain and develop chronic inflammation and anemia due to functional iron deficiency. For the treatment of mild to moderate pain, non-opioid analgesic compounds are widely used.[1] Diclofenac (DCF) and acetaminophen (APAP/paracetamol) are common over-the-counter drugs with analgesic, antipyretic, and anti-inflammatory effects, acting through inhibition of prostaglandin synthesis. DCF directly binds to and inhibits cyclooxygenases (COX)-1 and -2.[2–4] APAP has been proposed to be metabolically converted and conjugated with arachidonic acid to N-arachidonoylaminophenol (AM404), thereby indirectly inhibiting COX.[5] Since prostaglandin synthesis affects the production of the key pro-inflammatory cytokine interleukin (IL)-6,[6] DCF and APAP may affect the IL-6-mediated acute-phase response.

IL-6 binds to the IL-6 receptor (IL-6R) and the signal transducer glycoprotein 130 (gp130), activating the receptor-associated Janus kinase 1 (JAK1) and leading to phosphorylation of gp130 and recruitment of the signal transducer and activator of

transcription (STAT)3. Phosphorylated STAT3 dimerizes, translocates to the nucleus, and activates target gene expression.[7] One early target gene of STAT3 is the suppressor of cytokine signaling 3 (SOCS3), which mediates receptor degradation and inhibition of JAK1, thereby shaping the extent and duration of the IL-6 response.[7] However, context-specific factors could in addition affect the dynamics of the negative feedback loop and, as a consequence, modulate IL-6 signaling responses.

In the liver, IL-6-induced STAT3 activation triggers the early, intermediate, or late expression of target genes encoding acute-phase response proteins.[8,9] A prominent acute-phase protein is hepcidin, which is encoded by the *HAMP* gene. Hepcidin, a key regulator of iron homeostasis, acts systemically: it is produced by hepatocytes and secreted into the bloodstream. By binding to the iron exporter ferroportin, it inhibits the uptake of dietary iron by duodenal enterocytes and the release of release from macrophages and hepatocytes.[10] Hepcidin expression is regulated not only by IL-6 but also by the bone morphogenic protein (BMP) pathway.[11] BMPs are signaling proteins of the transforming growth factor β (TGF-β) superfamily and are primarily secreted by non-parenchymal cells in the liver such as hepatic stellate cells[12] or liver sinusoidal endothelial cells.[13] Binding of BMP ligands to type I and II BMP receptors (BMPRs) activates phosphorylation of mothers against decapentaplegic homolog 1 (SMAD1), 5 and 8 and their complex formation with SMAD4.[14] The resulting SMAD-complexes translocate to the nucleus and induce target gene expression, including inhibitor of DNA binding 1 (ID1) and 3 (ID3).[15] BMP signal transduction is inhibited by the induction of the feedback regulators SMAD6 and SMAD7,[16–18] extracellular antagonists such as Noggin[19] or small-molecule inhibitors, including dorsomorphin that target type I BMPRs,[20] providing means for targeted modulation of hepcidin expression.

Given that cancer patients frequently take high doses of DCF and APAP, a systematic elucidation of differences in their responses is of clinical relevance. Hepatotoxic effects of DCF and APAP at extended exposure times and escalating dosages indicate potential effects on the global proteome of liver cells.[21] These observations suggest that both drugs might have global effects on the proteome of liver-derived cells and thus could affect the IL-6 mediated induction of acute-phase proteins. As differences in protein synthesis, metabolism, transport, and drug metabolism exist between hepatoma cell lines and primary human hepatocytes (PHHs),[22] DCF and APAP might have distinct effects in these cellular model systems.

A key aspect could be to address the molecular mechanisms determining the impact of DCF and APAP on the induction of IL-6 mediated responses and potential cross-talks with other pathways such as BMP signal transduction. Due to the non-linearity of the involved reactions and feedback regulation, a mathematical modeling approach is required to systematically elucidate regulatory mechanisms[23] and to identify reactions affected by compounds such as DCF and APAP. Several mathematical models of the IL-6 pathway have been developed.[9] These models were utilized to dissect the contribution of the combinatorial binding of STAT3 and SMAD-complexes to the *HAMP* mRNA promoter region, and to quantify the impact of IL-6 and BMP signal transduction on hepcidin expression.[11] By the establishment of the L_1-regularization approach that allows to identify cell-context-specific reactions in a signaling network,[24] we provide the means to systematically pinpoint reactions in the complex IL-6 signal transduction network potentially affected by DCF and APAP.

Here, we show that the non-opioid analgesics DCF and APAP reduce the expression of acute-phase proteins in the hepatoma cell line HepG2 and PHHs. Using data-based mechanistic modeling, we dissect the effects of DCF and APAP on IL-6 and BMP signal transduction as well as their integrative impact on hepcidin expression in both cell types, and provide insights into the inter-patient heterogeneity of the regulation. This approach allows us to identify a mechanism leading to an amplified expression of hepcidin in hepatoma cells. Validation of the cell-context-specific mechanism allows to propose a selective intervention strategy that could be employed to counteract the adverse impact of the widely used pain-relieving drugs on iron homeostasis in liver cancer.

RESULTS

Quantitative proteomics reveals the impact of DCF and APAP on the acute-phase response in liver cells

To evaluate the potential impact of the non-opioid analgesics DCF and APAP on signal transduction induced by IL-6 in liver cells, we conducted a system-wide proteomic analysis of PHHs and the human hepatoma cell line HepG2 stimulated with 10 ng/mL IL-6 for 6 h. This IL-6 concentration was selected since it resulted in maximal phosphorylation of STAT3, the key mediator of IL-6 signal transduction, in both cell types (Figures S1A and S1E). Using data independent acquisition (DIA)-mass spectrometry (MS) (Figures 1A and 1C), we detected approximately 6,000 proteins in PHHs (Figure S1B), of which 1,200 proteins were decreased and 600 were increased in response to IL-6 (based on uncorrected p value < 0.05, Figure S1C). In HepG2 cells, about 8,000 proteins were detected (Figure S1F), of which about 300 proteins were decreased and 150 proteins were increased (uncorrected p value < 0.05), suggesting that overall IL-6 responsiveness was higher in PHHs compared with HepG2 cells, although present in both cell types. To identify biological processes modulated by IL-6 stimulation, we applied ingenuity pathway analysis (IPA)[25] and identified the acute-phase response to be among the most significantly upregulated pathway upon IL-6 stimulation in PHHs and the most upregulated pathway in HepG2 cells (Figures S1D and S1H).

A more detailed analysis of the acute-phase response associated proteins detected in our global proteome study revealed that in PHHs, the majority of known IL-6-induced acute-phase proteins were detected, with the exception of SOCS3, hepcidin, and factor 8 (F8) (Figure 1B), which is most likely due to their low abundance. In PHHs, more than half of the detected acute-phase proteins were significantly increased after 6 h of IL-6 stimulation, including serum amyloid P-component (APCS), C-reactive protein (CRP), heme oxygenase 1 (HMOX1) and 2 (HMOX2), haptoglobin (HP), lipopolysaccharide-binding protein (LBP), alpha-1-antiproteinase (SERPINA1), superoxide dismutase [Mn], mitochondrial (SOD2), and fibrinogen chains alpha (FGA), beta (FGB), and gamma (FGG) (Figures 1B and S1C). In HepG2 cells, we detected fewer IL-6-induced acute-phase

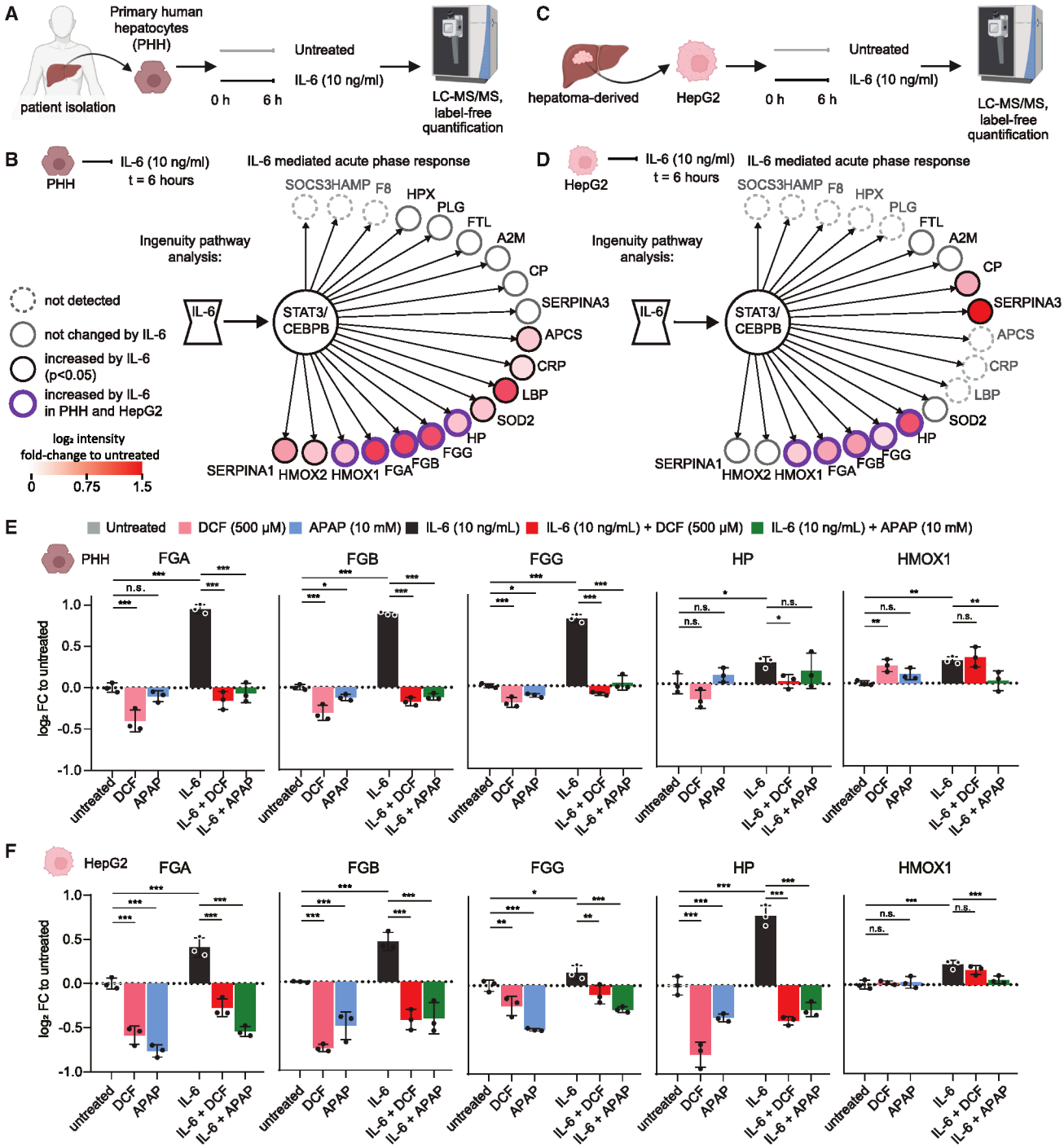

Figure 1. DCF and APAP globally downregulate proteins of the acute-phase response in hepatic cells

(A) Experimental approach for the analysis of IL-6-induced proteome changes in primary human hepatocytes (PHHs) by data independent acquisition (DIA).

(B) Whole proteome data of IL-6-treated non-cancerous PHH from one donor (for more information see Table 1, patient 1) were functionally enriched for IL-6-mediated acute-phase proteins (APPs) based on the ingenuity pathway knowledge base. *Limma t* test statistics identified APPs significantly increased ($p < 0.05$) compared with untreated control cells. $n = 3$.

(C) Experimental approach for the analysis of IL-6-induced proteome changes in HepG2 cells.

(D) Whole proteome data of IL-6-treated HepG2 ($n = 3$) cells were enriched for IL-6-mediated APPs as in (B).

(E and F) (E) PHH and (F) HepG2 data on the effect of DCF and APAP on the APPs identified to be increased by IL-6 in both cell types (purple in B and D). Cells were treated with the indicated compounds for 6 h and analyzed by DIA. Bars represent mean ± SD, $n = 3$. Significance was calculated by ordinary one-way ANOVA with Benjamini, Krieger and Yekutieli correction with an FDR of 5%. n.s., not significant, $^{*}p < 0.05$, $^{**}p < 0.01$, $^{***}p < 0.001$, $n = 3$.

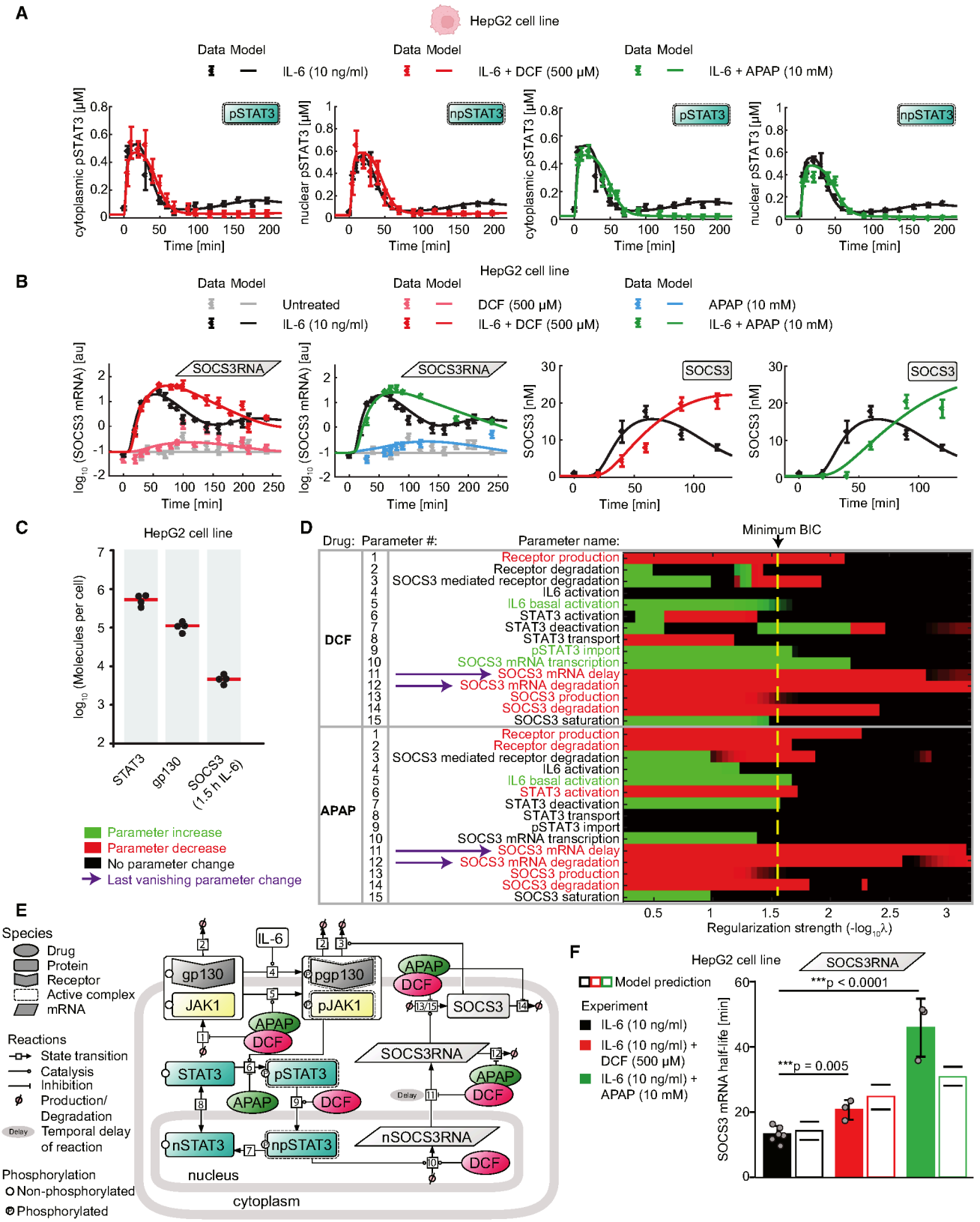

(legend on next page)

proteins; however, similar to what we observed in PHHs, FGA, FGB, FGG, HMOX1, and HP, as well as ceruloplasmin (CP) and alpha 1-antichymotrypsin (SERPINA3), were increased by IL-6 stimulation (Figures 1D and S1G), establishing these proteins as key markers for the IL-6-induced acute-phase response in our liver cell models.

To evaluate the impact of DCF or APAP on IL-6 induced responses in PHH and HepG2 cells, we employed 500 μM DCF and 10 mM APAP for 6 h. This choice was based on own experiments,[26] and the results of a ring trial[21] showing that exposure to doses of 1 mM DCF and 30 mM APAP for 24 h were tolerated by PHH and HepG2 cells but had a hepatotoxic effect after 72 h of exposure. Furthermore, we confirmed in a dose escalation study with HepG2 cells that a 3-h exposure with the selected doses (Figure S3A) did not result in hepatotoxic effects, as determined by overall changes in mRNA expression. Accordingly, at the global proteome level, we detected by DIA-MS in PHH and HepG2 cells stimulated with IL-6, DCF, APAP, or co-treated for 6 h equal numbers of proteins (Figure S2), indicating that no general toxicity was induced within this time frame, thereby avoiding bias in our analysis. Of note, treatment with DCF or APAP alone already had a global effect on protein abundance compared with the DMSO control: in PHH, a decrease in about 1,100 proteins and an increase in about 600 proteins was observed (Figure S2A), and for HepG2 cells, the effects were even more pronounced as about 1,800 proteins were decreased and 800 were increased (Figure S2C).

Given the impact at the global proteome level, we hypothesized that both compounds could affect the IL-6-induced acute-phase response. To define the influence and determine whether DCF and APAP have distinct roles, we focused our analysis on the acute-phase marker proteins FGA, FGB, FGG, HMOX1, and HP, since they are induced by IL-6 stimulation in both cell types, yet to a stronger extent in PHH compared with HepG2 cells (Figures S1C and S1G). In both cell types, DCF or APAP alone led to a reduction of the control levels of FGA, FGB, and FGG but had a stronger inhibitory effect on the IL-6-induced expression (p value < 0.001) of these proteins (Figures 1E and 1F). In PHH, the induction of HP and HMOX1 in response to IL-6 stimulation was less pronounced compared with the other examined marker proteins, but upon co-treatment with DCF, HP levels were significantly reduced, and upon APAP treatment, HMOX1 expression was lowered. HepG2 cells displayed a similar inhibitory effect of DCF and APAP on the expression of FGA, FGB, FGG; however, in these cells, the expression of HP was also strongly induced by IL-6 and inhibited by APAP or DCF (Figure 1F).

Thus, our global proteome studies identify PHH and HepG2 as suitable cellular models to study IL-6-induced acute-phase responses. We demonstrate that already after 6 h of exposure, the non-opioid analgesics DCF and APAP inhibit the expression of acute-phase proteins.

DCF and APAP decrease long-term IL-6 responses by increasing *SOCS3* mRNA half-life

To systematically unravel mechanisms explaining the inhibitory effects of DCF and APAP on the IL-6-induced acute-phase responses in PHH and HepG2, we first studied the impact of both compounds on the IL-6 signal transduction pathway in HepG2 cells, since the availability of PHHs is very limited.

Time-resolved stimulation of HepG2 cells with IL-6 for up to 3 h led to a transient increase of phosphorylated STAT3 in the cytoplasm (pSTAT3) and the nucleus (npSTAT3), reaching a maximum amount of 0.55 μM (pSTAT3) and 0.65 μM (npSTAT3) after 10 min and returning to steady-state levels of around 0.1 μM after 70 min (Figure 2A, symbols). Co-stimulation with IL-6 and DCF or APAP did not affect the time-to-peak nor the peak amplitude but resulted in reduced levels of pSTAT3 and npSTAT3 beyond 60 min of co-stimulation compared with non-drug treated cells. The induction of the mRNA and protein of the negative feedback regulator SOCS3 reached a peak between 50 and 60 min (Figure 2B, symbols). Co-treatment with IL-6 and DCF or APAP prolonged the peak of *SOCS3* mRNA expression, delayed its peak expression by approximately 10 min, and led to a more linear decline back to steady-state levels. Even though DCF and APAP delayed the initial SOCS3 protein expression, its absolute abundance increased over 120 min of IL-6 stimulation, providing a possible explanation for the reduced STAT3 levels after prolonged DCF or APAP treatment.

To further elucidate the molecular mechanism that might contribute to the observed effects of DCF and APAP on IL-6 signal transduction, we established a mathematical model

Figure 2. DCF and APAP decrease long-term IL-6 responses by increasing *SOCS3* mRNA half-life

(A) Experimental data (symbols) of nuclear and cytoplasmic pSTAT3 in HepG2 cells treated with the indicated compounds and respective model trajectories (lines). Shown are mean ± SD, $n = 3$. Model trajectories were generated with the IL-6 core model with drug-modified parameters shown in (E). Error bars are based on uncertainty estimated by the error model, based on triplicates.

(B) Experimental data (symbols) of *SOCS3* mRNA and SOCS3 protein expression in HepG2 cells treated with the indicated compounds and model trajectories (lines). mRNA amounts measured by quantitative real-time polymerase chain reaction were normalized to the housekeeper *HPRT*. Shown are mean ± SD, $n = 3$. Model trajectories were generated as in (A).

(C) Number of molecules per cell of STAT3 and gp130 in untreated HepG2 cells and of SOCS3 in IL-6 treated HepG2 cells determined by quantitative immunoblotting ($n = 4$, average indicated by red line).

(D) L_1-regularization was used to identify parameter changes that are required in the mathematical core model from (E) to describe the drug effect of DCF and APAP. Data shown in (A) and (B) were employed for calculating the Bayesian information criterion (BIC). The yellow line indicates the minimum of the BIC used to select which parameter differences are important to describe the data. Purple arrows indicate the two most crucial parameter changes.

(E) IL-6 core model including the effect of DCF and APAP on the different reactions. BIC calculations of the L1 regularization (D) were employed to determine the essential parameters reflecting the impact of DCF and APAP. These parameters were included in the model reactions. Arrows indicate biochemical reactions and represent ordinary differential equations (ODEs). Phosphorylated species are indicated by P. Model topology was developed based on the mathematical model presented in Sobotta et al.[9]

(F) Model-predicted (striped bars) and quantitative real-time polymerase chain reaction measured (solid bars) effect of DCF and APAP on IL-6 dependent *SOCS3* mRNA half-life. Confidence intervals are indicated by horizontal black lines. mRNA half-lives were calculated from three independent experiments. Bars represent mean ± SD, $n = 3$. Significance was tested with Student's t test, n.s., not significant, $^{*}p < 0.05$, $^{**}p < 0.01$, $^{***}p < 0.001$.

(Figure 2E) based on our previously reported mechanism-based dynamic pathway model of IL-6 induced JAK1/STAT3 signal transduction in primary murine hepatocytes (PMHs).[9] Here, we focus on the gp130/JAK1 receptor complex, the different phosphorylated species of STAT3, as well as *SOCS3* mRNA and SOCS3 protein, with the final IL-6 core model consisting of 12 coupled ordinary differential equations (ODEs) (Methods S2.1.3). To calibrate the mathematical model, we measured the absolute concentrations of receptor, transcription factor, and negative feedback protein by quantitative immunoblotting, showing that HepG2 cells contain approximately 528,000 STAT3 molecules/cell and 108,000 gp130 molecules/cell in absence of IL-6 and 5,000 SOCS3 molecules/cell upon stimulation with IL-6 for 90 min (Figure 2C). The obtained abundances were converted to cellular concentrations based on a total cell volume of 850 μm^3 and a nuclear:cytoplasmic ratio of 1:3 for HepG2 cells.[22] The three parameters describing the degradation rate of the IL-6 receptor complex were derived from Gerhartz et al.[27] The remaining 15 dynamical parameters of the IL-6 core model were estimated based on our experimental time course data obtained in HepG2 cells (Figures 2A and 2B).

To systematically identify potential molecular targets of DCF and APAP in the IL-6 signal transduction network, we employed the mathematical model to investigate which of the 18 dynamical parameters of the IL-6 core model were changed in the presence of DCF or APAP. Therefore, we performed an L_1-regularization approach,[24,26] which identified the minimal set of parameters that had to be adjusted in the drug-treated conditions to match the mathematical model with the experimental data. Figure 2D displays the model-predicted changes of these parameters in the presence of DCF or APAP as a function of the regularization strength. By calculating the Bayesian information criterion (BIC), we identified the regularization strength indicating a parsimonious model (dashed yellow line in Figure 2D), indicating the smallest number of parameters that are required to be changed while the model is still in line with the experimental data. This analysis revealed a set of eight key parameter changes per drug in the reaction network. Compared with IL-6-treated samples, treatment with DCF required five parameters to be decreased (red) and three parameters to be increased (green, Figure 2D, upper), whereas APAP required seven parameters to be decreased and one parameter to be increased (Figure 2D, lower). The significance of the APAP- and DCF-mediated differences was determined by calculating the likelihood profiles of the L_1 model, as shown in Figure S8. Concluding, the L_1-regularization approach predicted an impact of DCF or APAP on IL-6 induced signal transduction in HepG2 cells based on the following model parameters: DCF decreases receptor production, delays the nuclear export of *SOCS3* mRNA, and decreases degradation of *SOCS3* mRNA, SOCS3 protein production, and degradation (Figure 2D, upper, red letters). Additionally, DCF also increases the basal activation of IL-6 signal transduction, as well as the nuclear import of pSTAT3 and *SOCS3* mRNA transcription (Figure 2D, upper, green letters). APAP decreases receptor production, receptor degradation, STAT3 activation, *SOCS3* mRNA degradation, as well as delays *SOCS3* mRNA transcription and, in turn, decreases SOCS3 protein production and degradation (Figure 2D, lower, red letters). Additionally, an increase in the basal activation of IL-6 signal transduction by APAP was predicted (Figure 2D, lower, green letters). Following L_1-regularization, we computed confidence intervals via the profile likelihood method[28] (see Figure S7 and Methods 2.2.2) and uncovered that, despite being selected in the analysis, the degradation effect of APAP on the IL-6 receptor was not necessary in the calibrated IL-6 model (Figure 2E). Altogether, the parameters of the final model, including the effect of DCF and APAP, were calibrated based on 1,484 data points. The calibrated IL-6 signal transduction model, including the predicted impact of DCF and APAP on IL-6 signal transduction, was able to describe the experimental data of IL-6 induced STAT3 phosphorylation upon drug treatment as well as the DCF- and APAP-dependent changes (Figure 2A, lines). Furthermore, it was also capable of capturing the sustained increase of *SOCS3* mRNA and the delayed increase in SOCS3 protein abundance upon co-treatment with IL-6 and DCF or APAP (Figure 2B, lines).

Intriguingly, six out of eight parameter changes were the same for both compounds, with *SOCS3* mRNA delay and degradation being consistently decreased throughout the regularization procedure with the highest regularization strength (Figure 2D, purple arrows). Accordingly, we predicted with our mathematical model that the half-life of the IL-6-induced *SOCS3* mRNA increased from 14.4 to 25.1 min upon co-stimulation with DCF and even to 31.2 min upon co-stimulation with APAP (Figure 2F, striped bars). To experimentally validate this model-predicted RNA-stabilizing effect of DCF and APAP, we measured *SOCS3* mRNA half-life in HepG2 cells either treated with IL-6 alone or in combination with IL-6 and one of the compounds. Indeed, DCF treatment increased *SOCS3* mRNA half-life in IL-6 treated cells nearly 2-fold, from 12.7 to 20.9 min, and APAP even nearly 4-fold, to 46.5 min (Figure 2F, solid bars).

Taken together, we show with our mathematical modeling approach that DCF and APAP affect multiple reactions in the IL-6 signal transduction network and identify an increase in the mRNA half-life of the key negative regulator *SOCS3* mRNA as the most prominent drug effect. Thus, the increased presence of the negative feedback loop upon co-treatment with DCF or APAP lowers STAT3 activity, which could explain the observed marked reduction in the IL-6 acute-phase response proteins in our proteome studies.

DCF and APAP activate the BMP signal transduction pathway in HepG2 cells

To disentangle the impact of DCF or APAP on the regulation of the expression of IL-6-induced acute-phase proteins, we measured IL-6-induced acute-phase target genes in HepG2 cells that we previously identified in our whole proteome analysis (Figure 1F) or in PMHs,[9] comprising *FGA*, *FGG*, *HAMP* mRNA, *HP* and *HPX*. IL-6 strongly induced the mRNA expression of *FGA*, *HAMP*, and *HP* in HepG2 cells. Co-treatment with DCF either had no effect on IL-6 induced target gene expression or slightly increased the expression of *FGA* and *HP*. APAP co-treatment had an inhibitory effect, particularly on *FGA* and *HP* expression (Figure 3A). The IL-6 induced expression of *HAMP* mRNA was the strongest among the examined candidates and was even further amplified after 60 min of co-treatment with either drug, with DCF having a stronger effect than APAP. Densely sampled time-resolved *HAMP* mRNA expression data from HepG2 cells stimulated with different IL-6, DCF, and APAP

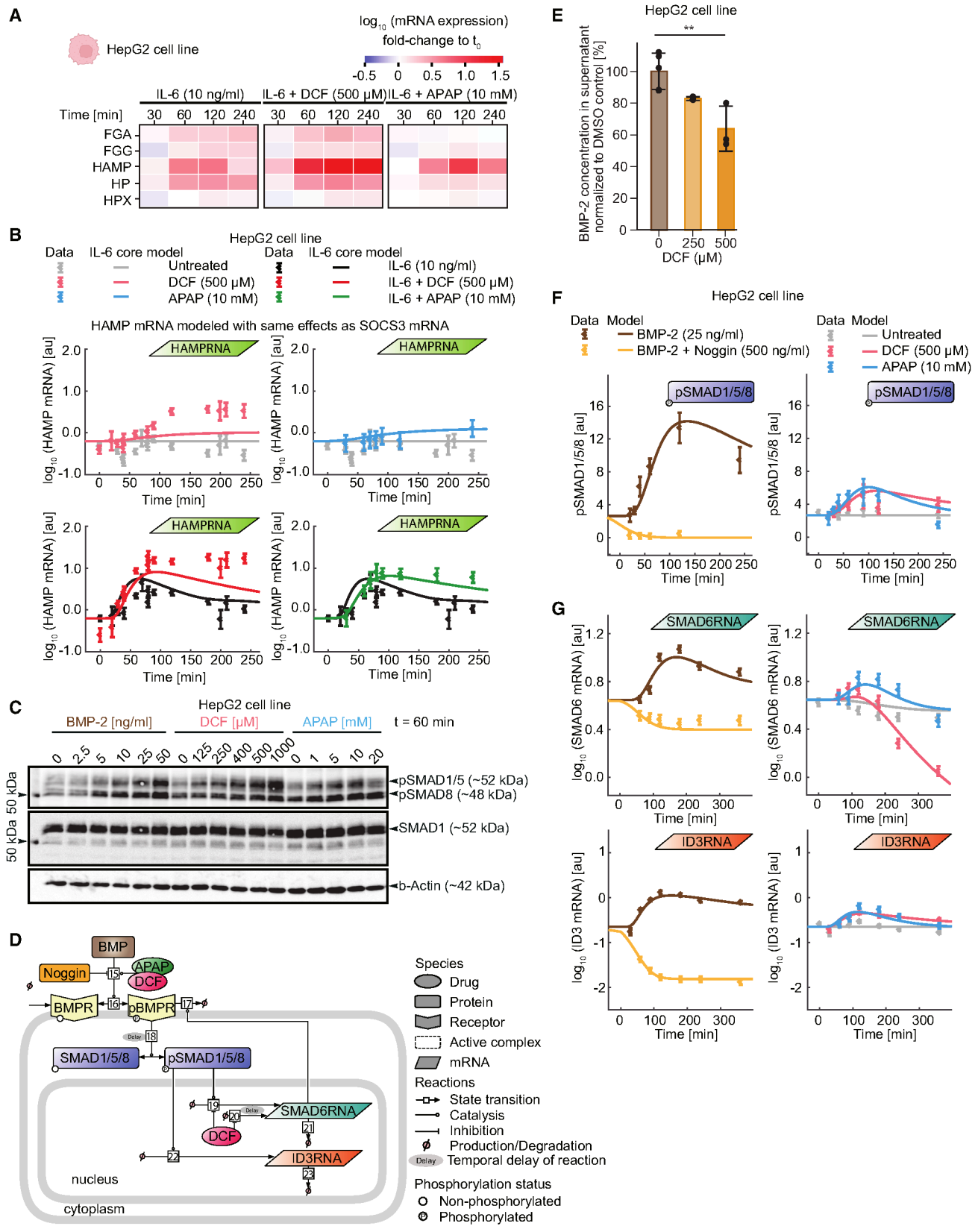

(legend on next page)

combinations (Figure 3B, symbols) revealed that *HAMP* mRNA expression was induced after approximately 25 min by IL-6, reaching its peak at 70 min, and returned to a steady state after approximately 180 min (Figure 3B, black symbols). Treatment with DCF alone resulted in an increase in *HAMP* mRNA after approximately 50 min, which reached a sustained peak after 120 min (Figure 3B, pink symbols). This effect was more than 2-fold higher upon co-stimulation with IL-6 and DCF (Figure 3B, red symbols). APAP treatment alone slightly induced *HAMP* mRNA expression only at late time points (Figure 3B, blue symbols). However, co-stimulation with IL-6 and APAP enhanced *HAMP* mRNA expression, albeit to a lower extent compared with the combination of IL-6 and DCF (Figure 3B, dark green symbols).

To evaluate whether the amplifying effect of the compounds is already detectable at lower compound concentrations, we performed a dose-response experiment testing the impact of 16 to 500 μM DCF and 0.3 to 10 mM APAP on IL-6 induced *HAMP* mRNA expression at 120 min (Figure S3B). The results showed that half-maximal amplification of *HAMP* mRNA expression was already reached at 153 μM DCF and 0.6 mM APAP, confirming that at 500 μM DCF and at 10 mM APAP amplifying effects were maximal. These findings support the conclusion that the expression-enhancing impact of the compounds on *HAMP* mRNA is robust and independent of potential hepatotoxic effects.

To extent our mathematical model to include the dynamics of *HAMP* mRNA, we employed the IL-6 core model (Figure 2E) with the same parameters used for describing *SOCS3* mRNA expression, except for gene-specific parameters to describe *HAMP* mRNA expression dynamics (Figure 3B). The mathematical model was able to capture the *HAMP* mRNA expression dynamics for IL-6 or APAP alone, as well as co-treatment with both; however, it failed to describe the increased and sustained levels of *HAMP* mRNA upon treatment with DCF alone (Figure 3B, pink line) or the strong acceleration and increase of *HAMP* mRNA upon IL-6 and DCF co-stimulation (Figure 3B, red line). This indicated that, in particular DCF, but also APAP, might not affect *HAMP* mRNA expression exclusively via the IL-6 pathway, but through additional regulation of a different signaling pathway. Since the BMP/SMAD pathway is another main regulator for hepcidin expression in the liver,[29] we investigated whether BMP/SMAD signaling in HepG2 cells was affected by DCF or APAP treatment. We observed basal phosphorylation of SMAD1/5/8 in HepG2 cells, which was enhanced with escalating doses of DCF (0–1,000 μM) and APAP (0–20 mM) to a comparable degree as upon stimulation with recombinant human BMP-2 (Figure 3C). Therefore, we developed a separate, simplified mathematical model to describe the BMP signal transduction cascade to investigate the effect of DCF or APAP on this pathway (Figure 3D; Methods S2.4). The variables of the BMP core model consisted of the BMPR complex, the downstream transcription factors SMAD1/5/8 in a trimeric complex, and the negative feedback regulator SMAD6. Phosphorylation of BMPR was maintained via basal levels of BMP. The activation of the BMP pathway by DCF and APAP was included by assuming that both compounds stabilize the binding of BMP ligands to the receptor. To confirm this model-based hypothesis, we performed a BMP depletion assay, assuming that compound-mediated stabilization of the ligand-receptor interaction would result in diminished ligand levels in the cell supernatant. Indeed, in the supernatant of HepG2 cells incubated with 2.5 ng/mL BMP2 alone or in combination with 250 or 500 μM DCF for 1 min, BMP2 levels significantly decreased in the presence of DCF. We selected 2.5 ng/mL BMP for the depletion experiment based on the observation that this concentration elicited SMAD1/5/8 phosphorylation but did not saturate the response (Figure 3C). We observed that 250 μM of DCF decreased BMP2 concentration in the medium to ∼85% compared with the control, which was further reduced to ∼65% by exposure to 500 μM DCF (Figure 3E, p value < 0.01). Additionally, we included the *ID3* as a target gene, which, unlike SMAD6, is not a negative feedback regulator of the BMP pathway but regulates the expression of other target genes. To calibrate the BMP core model, we experimentally measured drug-induced SMAD1/5/8 phosphorylation dynamics as well as gene expression levels in HepG2 cells either treated with BMP-2 alone, pre-treated with the BMP antagonist Noggin

Figure 3. DCF and APAP activate the BMP signal transduction pathway in HepG2 cells

(A) Impact of DCF or APAP on the expression of APP genes in HepG2 cells. mRNA expression of indicated genes was normalized to the housekeepers *HPRT*, *GAPDH*, and *TBP*. Independent experiments (n = 3) were scaled to each other using a mixed-effect model within the *blotIt2* package in R, and fold-change relative to the unstimulated control at the start of the experiment (t = 0 min) was calculated.

(B) Experimental data (symbols) of *HAMP* mRNA expression dynamics in HepG2 cells treated with the indicated compounds and respective model trajectories (lines). *HAMP* mRNA expression was normalized to the housekeepers *HPRT* and *GAPDH*. Model trajectories were generated with the IL-6 core model from Figure 2E. Error bars are estimated by the error model based on triplicates.

(C) Dose response of BMP-2, DCF, and APAP on SMAD1/5/8 phosphorylation in HepG2 cells. HepG2 cells were treated with increasing concentrations of BMP-2, DCF, or APAP, and pSMAD1/5/8, SMAD1, and β-actin detected with quantitative immunoblotting.

(D) BMP signal transduction model including the effect of DCF and APAP on different parameters. Arrows indicate biochemical reactions and represent ODEs. Phosphorylated species are indicated by P.

(E) BMP2 depletion from the experimental medium detected with a multiplexed immunoassay kit. HepG2 cells were treated with different concentrations of DCF (0 mM: brown, 250 mM: light orange, 500 mM: dark orange) for 30 min. Then, 2.5 ng/mL BMP2 was added to the medium, and after 1 min, BMP2 concentration in the supernatant was detected. Data are presented as individual replicates, bars represent mean ± SD. Statistical significance was assessed using the Kruskal-Wallis test followed by Dunn's post hoc test for multiple comparisons due to non-normal distribution and unequal variances across groups (n.s., not significant, $^{*}p < 0.05$, $^{**}p < 0.01$, $^{***}p < 0.001$, n = 3).

(F) Experimental data (symbols) of SMAD1/5/8 phosphorylation dynamics in HepG2 cells upon stimulation with the indicated compounds determined by quantitative immunoblotting and respective model trajectories (lines). Model trajectories were generated with the BMP signal transduction model from (D). Error bars are based on uncertainty estimated by the error model based on triplicates.

(G) Experimental data (symbols) of *SMAD6* and *ID3* mRNA expression dynamics in HepG2 cells upon stimulation with the indicated compounds and respective model trajectories (lines). mRNA expression was normalized to the housekeepers *HPRT* and *GAPDH*. Model trajectories were generated as in (F).

followed by subsequent BMP-2 stimulation, or treated with DCF or APAP alone (Figures 3F and 3G, symbols). As expected, treatment with BMP-2 induced a strong, transient increase in SMAD1/5/8 phosphorylation (Figure 3F, brown symbols), which was reduced below baseline levels by pre-treatment with Noggin, indicating basal activation of BMP signal transduction in HepG2 cells (Figure 3F, yellow symbols). In line with the results presented in Figure 3C, both DCF (Figure 3F, pink symbols) and APAP (Figure 3F, blue symbols) induced a transient increase in SMAD1/5/8 phosphorylation in the absence of exogenous BMP stimulation. Quantification at the mRNA level confirmed that BMP-2 induced expression of *SMAD6* and *ID3* mRNA is suppressed below basal levels upon Noggin pre-treatment (Figure 3G, left). A comparable effect on *ID3* could be observed for DCF and APAP treatment (Figure 3G, bottom, pink and blue symbols). *SMAD6* gene expression was increased by APAP but strongly decreased upon prolonged DCF treatment (Figure 3G, top, pink and blue symbols). We calibrated the BMP signal transduction model based on the obtained experimental data and evaluated the parameters using the profile likelihood method<u>[28,30]</u> (Figure S9). Since 25 ng/mL BMP-2, as well as both 500 μM DCF and 10 mM APAP, induced SMAD1/5/8 phosphorylation to comparable degrees (Figure 3C), activation levels were set to be directly proportional to the corresponding activator. Interestingly, an explicit delay from receptor to pSMAD1/5/8 was required in the model, indicating that, while delayed, activation of pSMAD1/5/8 corresponds to a relatively rapid increase.

The observed reduction in *SMAD6* mRNA in response to DCF treatment (Figure3G) could only be captured by the model if an inhibitory effect of DCF on *SMAD6* mRNA expression was added. With these adaptations, the BMP signal transduction model was able to describe the transient activation of pSMAD1/5/8, *SMAD6*, and *ID3* mRNA upon BMP-2 treatment, as well as the decrease below baseline levels in response to a pre-treatment with Noggin (Figures 3F and 3G, lines; Methods S2.4.1). At the same time, it was able to capture the transient increase in SMAD1/5/8 phosphorylation and *ID3* expression upon treatment with DCF and APAP, as well as the increase of *SMAD6* mRNA upon APAP treatment and its decrease upon DCF addition.

In summary, our studies show that in HepG2 cells, DCF and APAP enhance IL-6-induced hepcidin expression, in contrast to other acute-phase proteins. Our approach suggests that DCF and APAP stimulate the binding of BMP ligands to the BMPR in HepG2 cells and that DCF inhibits the expression of *SMAD6* mRNA.

IL-6 and BMP signal transduction jointly regulate *HAMP* mRNA expression in hepatocellular carcinoma cells

Based on the insights gained with our mechanism-based mathematical models, we hypothesized that *HAMP* mRNA expression in HepG2 cells is cooperatively regulated by the IL-6 and BMP pathway. To investigate the individual influence of both pathways on *HAMP* mRNA expression after drug treatment, we performed time course analysis of HepG2 cells treated with different cytokine-compound-inhibitor combinations. Even though IL-6-induced expression of *HAMP* mRNA began approximately 25 min post stimulus addition, its gene expression reached a moderate peak around 70 min and subsequently returned to steady-state levels (Figure 4A, black symbols). In comparison, BMP-2-induced *HAMP* mRNA expression was delayed, starting after 60 min but was nearly three times as strong as observed for IL-6-induced expression, reaching a sustained plateau phase after roughly 180 min (Figure 4A, brown symbols). Next, we analyzed whether BMP pathway activity directly influences IL-6-mediated *HAMP* mRNA expression by pre-treating HepG2 cells with the BMP inhibitor Noggin, followed by IL-6 and DCF treatment. Interestingly, the previously observed additive effect of IL-6 and DCF co-treatment (Figure 4B, red symbols), which mimicked BMP-2-induced *HAMP* mRNA expression, was reduced down to IL-6 stimulation levels by Noggin pre-treatment (Figure 4B, purple symbols). The effect of Noggin was even stronger on APAP enhanced IL-6 induced *HAMP* mRNA expression (Figure 4C, green symbols), which was completely inhibited down to baseline levels (Figure 4C, dark blue symbols). These results indicate two possibilities: either the BMP pathway regulates *HAMP* mRNA expression by directly regulating IL-6 pathway activity or *HAMP* mRNA expression is regulated by both pathways independently, which in turn are regulated at different levels by DCF or APAP. We first investigated whether the IL-6 and DCF/APAP co-induced *SOCS3* mRNA expression is affected by BMP-2 or Noggin. Neither treatment of unstimulated HepG2 cells with BMP-2 (Figures 4D and 4E, brown symbols) nor pre-treatment with Noggin had any influence on *SOCS3* mRNA expression dynamics in response to IL-6 and DCF (Figure 4D, purple symbols) or APAP co-treatment (Figure 4E, blue symbols), ruling out a direct influence of BMP pathway activity on IL-6 signal transduction. Therefore, we postulated an independent but cooperative effect of both pathways on *HAMP* mRNA expression, with pathway regulation occurring at different levels by DCF or APAP. To investigate this mechanism, we developed an integrative pathway model, which unified our IL-6 and BMP core models and converged at the level of *HAMP* mRNA expression (Figure 4F). The integrative model contained all possible drug effects previously identified by our model-based approach, with additional inhibition of *HAMP* mRNA degradation by DCF and APAP, as well as a delayed export of nuclear *HAMP* mRNA by APAP, which also represents transcription and maturation. Additionally, experimental data and model analysis showed that *SOCS3* mRNA is not affected by the BMP-induced signal transduction module. Altogether, the integrative model was calibrated with all experimental data presented in Figures 2, 3, and 4, containing 4,549 data points in total, and was able to describe the acquired experimental data obtained in HepG2 cells. It captured the early induction of *HAMP* mRNA by IL-6 (Figure 4A, black lines) and the delayed induction by BMP-2 (Figure 4A, brown lines), as well as the synergistic increase in *HAMP* mRNA in response to drug-cytokine combinations and the reduction by Noggin pre-treatment (Figures 4B and 4C, lines). This substantially improved the model trajectories in comparison with the initial core model in Figure 3B. The integrative model also captured that neither BMP-2 nor Noggin impacted *SOCS3* mRNA expression (Figures 4D and 4E, lines).

In summary, we identify a BMP-dependent impact of DCF and APAP on IL-6 mediated *HAMP* mRNA expression in HepG2 cells and hypothesize, based on our integrative mechanistic mathematical model and experimental results, that DCF and APAP

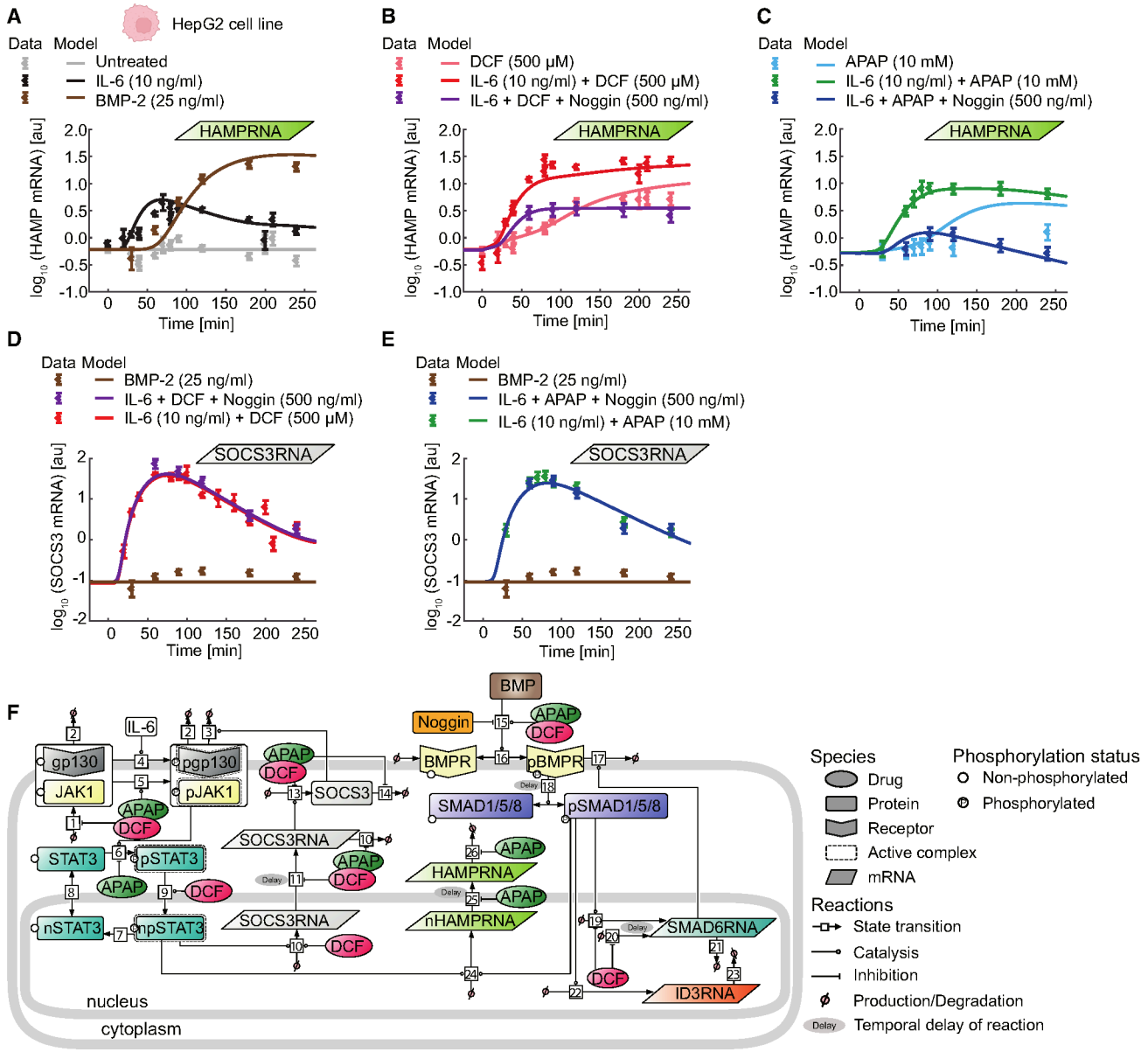

Figure 4. IL-6 and BMP signal transduction jointly regulate *HAMP* mRNA expression in hepatocellular carcinoma cells

(A–C) Experimental data (symbols) of *HAMP* mRNA expression dynamics in HepG2 cells treated with the indicated compounds and respective model trajectories (lines). *HAMP* mRNA expression was normalized to the housekeepers *HPRT* and *GAPDH*. Model trajectories were generated with the integrative IL-6/STAT-BMP/SMAD model from (F). Error bars are based on uncertainty estimated by the error model based on triplicates.

(D and E) Experimental data (symbols) of *SOCS3* mRNA expression dynamics in HepG2 cells treated with the indicated compounds and respective model trajectories (lines). *SOCS3* mRNA expression was normalized to the housekeeper *HPRT*. Model trajectories were generated as in (A).

(F) Schematic representation of the integrative IL-6/STAT-BMP/SMAD model. Arrows indicate biochemical reactions and represent ODEs. Phosphorylated species are indicated by P. The IL-6 core model and the BMP signal transduction module were integrated and converge into the expression of *HAMP* mRNA.

enhance BMP ligand binding to the receptor in the hepatoma cell line HepG2 cells.

DCF- and APAP-induced *HAMP* mRNA expression depends on autocrine BMP signaling in hepatocellular carcinoma cells

The observation that DCF and APAP induced *HAMP* mRNA expression in HepG2 cells even in the absence of BMP stimulation, and that pre-treatment with the BMP pathway inhibitor Noggin inhibited BMP-induced SMAD1/5/8 phosphorylation below basal levels, suggested the presence of an autocrine BMP-secretion loop in HepG2 cells. Due to the differences that we observed at the proteome level (Figure 1), we speculated that this potential secretory loop might be absent in non-cancerous PHHs.

Therefore, we analyzed the supernatants of PHH and HepG2 cells, measuring the absolute concentrations of secreted

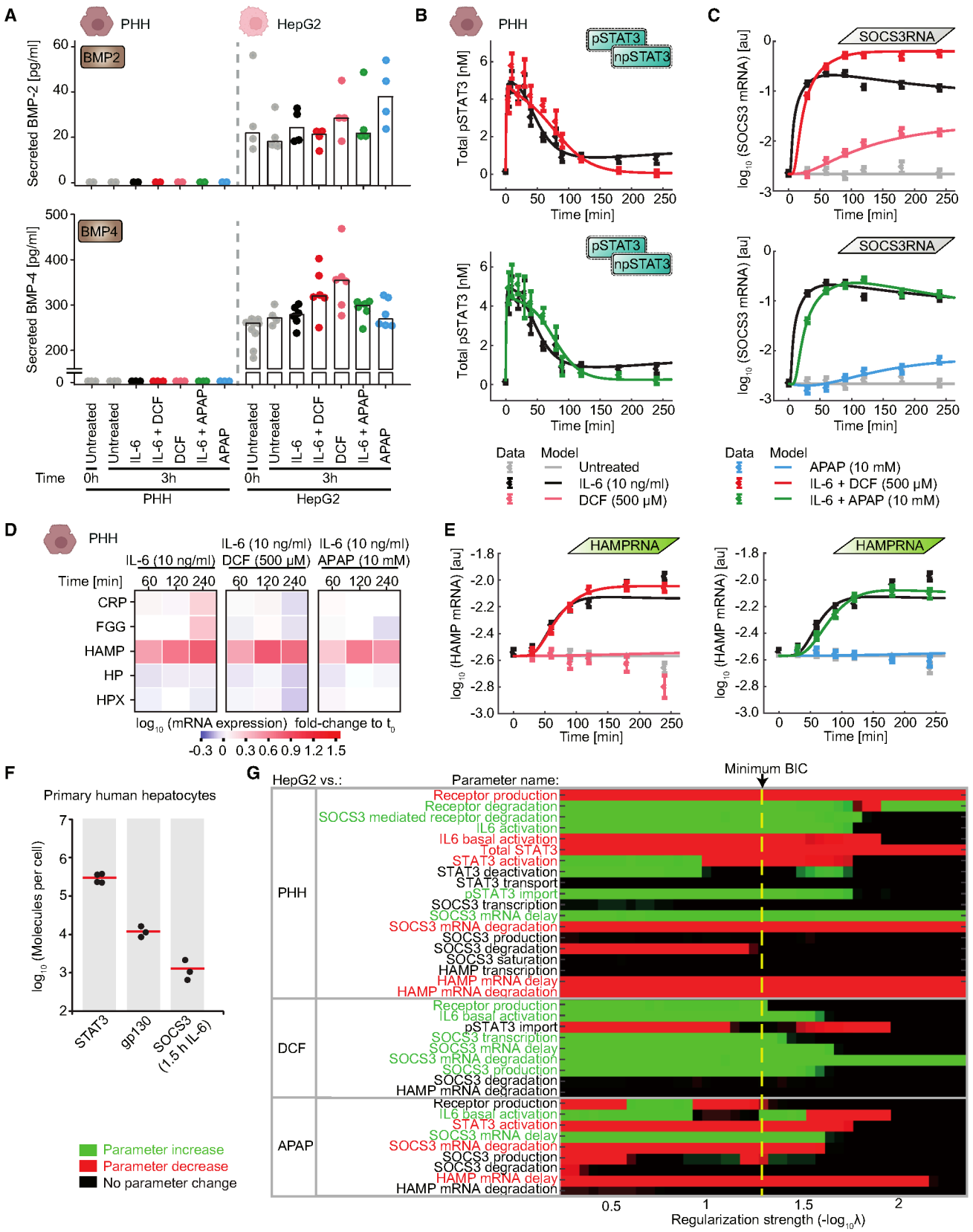

(legend on next page)

BMP-2, BMP-4, and BMP-6 ligands by ELISA after 3 h of treatment with different compounds or under untreated conditions. BMP-6 was not detectable in the supernatant of either cell system (thus data not shown). In the supernatants of PHH, neither basal levels nor IL-6/drug-stimulated secretion of BMP-2 or BMP-4 ligands was detectable (Figure 5A, left side). In untreated and treated HepG2 cells, we detected approximately 25 pg/mL of BMP-2 and 250 pg/mL of BMP-4 at the time of stimulation and after 3 h (Figure 5A, right side). These data confirmed that an autocrine BMP-secretion loop exists in HepG2 cells but is absent in PHH. This autocrine BMP secretion explains the observed basal phosphorylation of SMAD1/5/8 in Figure 3C. Treatment of cells with DCF or APAP or co-treatment with IL-6 did not significantly affect the amount of secreted BMP ligands in HepG2 cells (Figure 5A).

These results suggested that in PHH, the level of *HAMP* mRNA expression is primarily regulated by IL-6 signal transduction, and that the DCF- and APAP-mediated impact on *HAMP* mRNA expression through the stabilization of the ligand-receptor interaction and thus induction of BMP signal transduction is absent in PHH. To specify the impact of both compounds in PHH and gain insights into underlying mechanisms, we utilized our model-based approach and first examined whether DCF and APAP have the same effect on the core IL-6 signal transduction responses in PHH as in HepG2 cells. We observed that the overall dynamics of STAT3 phosphorylation in PHH was comparable to HepG2 cells, yet maximal phosphorylation was reached slightly faster, with a peak at ∼5 min after stimulation (Figures 2A and 5B), and with a more prolonged peak time of STAT3 phosphorylation upon DCF or APAP co-treatment, followed by a slower decline and similarly decreased steady-state levels as in HepG2 cells (Figure 5B, red and green symbols). While the IL-6 induced fold-induction of mRNA of the negative feedback regulator *SOCS3* in PHH was comparable to HepG2 cells (PHH ∼2.2 and for HepG2 ∼2.5), we observed, distinct from the transient SOCS3 expression in HepG2 cells (Figure 2B), a faster increase in *SOCS3* mRNA levels in PHH, which remained elevated for the entire observation time of 240 min (Figure 5C, black symbols). DCF co-treatment led to slightly delayed but even higher and more sustained levels of *SOCS3* mRNA in PHH (Figure 5C, red symbols), whereas the effect of IL-6 and APAP co-treatment in PHHs was comparable to IL-6 treatment alone (Figure 5C, green symbols). Furthermore, treatment with DCF or APAP alone also stimulated *SOCS3* expression in PHH (Figure 5C, pink and blue symbols), but to a higher extent than in HepG2 cells (Figure 2B). These experimental findings indicated the presence of a sustained negative feedback loop in PHH that is enhanced by DCF and APAP and thus affects the regulation of the core IL-6 signal transduction in PHH.

Next, we determined in PHH the impact of DCF and APAP on the dynamics of IL-6 induced mRNA expression of the acute-phase response genes *CRP*, *FGG*, *HAMP* mRNA, *HP*, and *HPX* (Figure 5D) that we had identified in our global proteome studies (Figure 1E). The mRNA expression of *CRP* and *FGG* started to increase at 240 min of IL-6 treatment and was, in line with the proteome analysis, inhibited by the addition of either DCF or APAP. Likewise, the mRNA expression of *HP* and *HPX* was further downregulated at 240 min of IL-6 and DCF co-treatment. Similar to HepG2 cells, IL-6 stimulation strongly induced the expression of *HAMP* mRNA but distinctively neither co-treatment with DCF or APAP had any effect on IL-6 induced *HAMP* mRNA expression, as opposed to the data observed in HepG2 cells. To gain further insights, we obtained densely sampled, time-resolved expression data of *HAMP* mRNA in PHH (Figure 5E, symbols). While in HepG2 cells DCF and APAP converted a transient IL-6-response to elevated and sustained expression of *HAMP* mRNA, in PHH, IL-6-induced *HAMP* mRNA expression reached a plateau at around 90 min and remained sustained over the observation time of 240 min (Figure 5E, black symbols). DCF or APAP had, on average, very little impact on *HAMP* mRNA expression in PHH (Figure 5E, red and green symbols).

Figure 5. DCF- and APAP-induced *HAMP* mRNA expression depends on autocrine BMP signaling

(A) Quantification of BMP ligand concentrations in cell culture supernatants. PHHs from at least two different donors ($n \geq 2$) (see Table 1 for patient information. *N*-number describes the number of different patients for this and all following analyses) and HepG2 ($n \geq 4$) cells were treated with the indicated compounds. Concentrations of secreted BMP-2 (upper) and BMP-4 (lower) in the supernatants were measured by ELISA or bead-based immunoassay, respectively. Individual experiments are shown as dots; mean values are indicated by bars.

(B) Experimental data (symbols) of STAT3 phosphorylation dynamics in PHH treated with the indicated compounds and respective model trajectories (lines). Model trajectories were generated with the IL-6/STAT-BMP/SMAD model from Figure 4F adapted to PHH. Error bars are based on uncertainty estimated by the error model based on quadruplicate determination ($n = 4$).

(C) Experimental data (symbols) of *SOCS3* mRNA expression dynamics in PHH treated with indicated compounds and respective model trajectories (lines). *SOCS3* mRNA expression was normalized to the housekeeper *HPRT*, *GAPDH*, *TBP*, and *GUSB*. Model trajectories and error bars were generated as in (B) based on quadruplicates ($n = 4$).

(D) Impact of DCF or APAP on the expression of selected APP genes in PHHs. mRNA of the indicated genes was measured by quantitative real-time polymerase chain reaction and values normalized to the housekeepers *HPRT*, *GAPDH*, and *GUSB*. Independent experiments ($n = 4$) were scaled to each other using a mixed-effect model within the *blotIt2* package in R and the fold-change to the unstimulated control at the start of the experiment (t = 0 min) was calculated.

(E) Experimental data (symbols) of *HAMP* mRNA expression dynamics in PHHs treated with the indicated compounds and analyzed as in (C). Model trajectories and error bars were generated as in (B) ($n = 7$).

(F) Molecules per cell of STAT3 and gp130 in untreated PHHs, and of SOCS3 in IL-6-treated PHHs determined by quantitative immunoblotting ($n = 3$–4, average indicated by red line).

(G) L_1-regularization was used to identify core parameters that are required in the integrative IL-6/STAT-BMP/SMAD model of PHHs, based on the model developed in HepG2 cells (Figure 4F) without modifying the model topology. Model parameters that had been estimated in HepG2 cells were iteratively compared with parameters obtained from multiple rounds of parameter estimation based on experimental data from PHHs (A, B, and D). These iterative comparisons were performed for the impact of APAP, DCF, and global differences between HepG2 and PHHs. Red: parameter required to describe the behavior in PHH was lower; green: parameter was higher; black: no parameter change necessary. The minimization of the BIC (indicated by arrow and yellow line) was used to select which parameter differences are important to describe the data in PHHs with the integrative IL-6/STAT-BMP/SMAD model (Figure SM30).

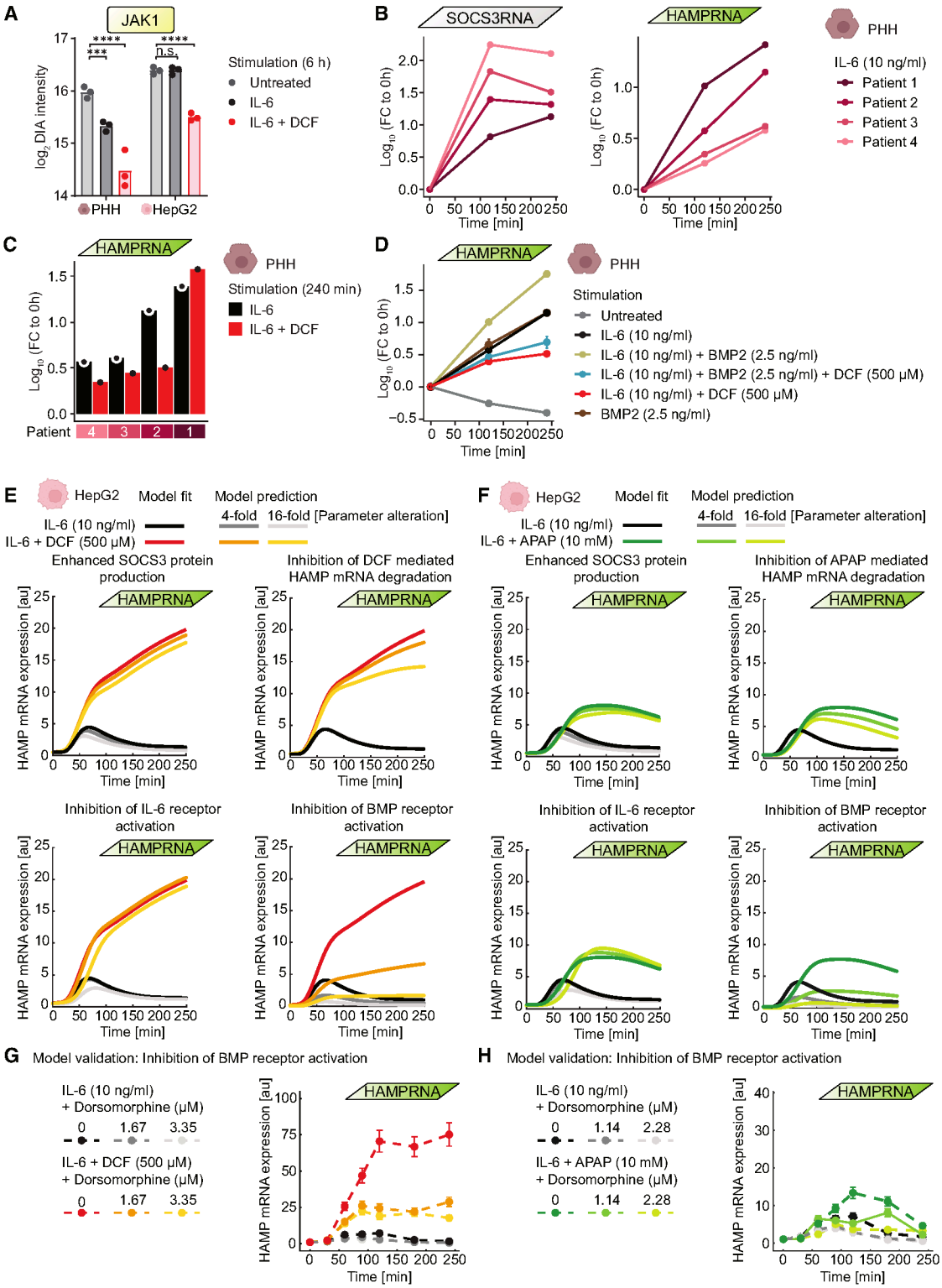

Figure 6. Inter-patient variability in *HAMP* mRNA expression in response to IL-6 and DCF co-stimulation and BMP pathway inhibition as intervention strategy

(A) Global proteome analysis showing JAK1 protein abundance in PHHs and HepG2 in response to IL-6 or IL-6 and DCF co-treatment. Data are presented as individual replicates. Bars represent mean values. Statistical analysis was performed using two-way ANOVA followed by Dunnett's post hoc test to compare each treatment group to the control. n.s., not significant, $^{*}p < 0.05$, $^{**}p < 0.01$, $^{***}p < 0.001$, $^{****}p < 0.0001$, $n = 3$.

(legend continued on next page)

Based on these insights, we adapted the structure of our integrative pathway model to PHH. The total amounts of STAT3 (297,700 molecules/cell), gp130 (12,000 molecules/cell), and SOCS3 (1,300 molecules/cell upon stimulation with IL-6 for 180 min) in PHH were determined by quantitative immunoblotting (Figure 5F) and converted to molecules per cell utilizing a cellular volume of PHH of 3,000 μm^3 with a nuclear:cytoplasmic ratio of 1:9.[22] Since PHH do not express BMP ligands and *HAMP* mRNA expression was not affected by DCF or APAP treatment in these cells, we only employed the IL-6 core model and the drug-mediated parameter changes on IL-6 signal transduction, as well as on *HAMP* mRNA expression. To determine parameters that are different in PHH compared with HepG2 cells, we again used L_1-regularization, using 1,075 data points for parameter estimation. This approach revealed the parameters that are altered in PHH compared with HepG2 cells (Figure 5G, top), as well as the DCF (Figure 5G, middle) or APAP (Figure 5G, bottom) induced parameter changes that are different in PHH. While most parameters had to be changed to adapt the HepG2-calibrated model to PHH, the model structure was sufficient to describe the experimental data without further alterations of the model topology. Using the profile likelihood method,[28] we computed confidence intervals, which identified that the major difference between PHH and HepG2 cells was the overall faster signal transduction dynamic in PHH e.g., a faster phosphorylation of the receptor by IL-6 stimulation or a shorter delay of *SOCS3* mRNA production upon IL-6 stimulation (see Methods S2.6.1). Intriguingly, while in HepG2 cells inhibition of *SOCS3* mRNA degradation by DCF was identifiable (parameter #29 in Figure S7), the parameter for the inhibition of SOCS3 degradation in PHH had an open-ended confidence interval toward positive values (parameter #19 in Figure S35), indicating that little to no *SOCS3* mRNA degradation takes place in the presence of DCF in PHH. The final model was able to accurately describe the experimentally observed effect of DCF and APAP on the IL-6 mediated STAT3 phosphorylation (Figure 5A, lines), as well as *SOCS3* (Figure 5B, lines) and *HAMP* mRNA expression dynamics in PHH (Figure 5E, lines).

In sum, our mechanism-based mathematical model identifies that in HepG2 cells and PHH, *HAMP* mRNA expression is regulated to a different extent by IL-6 as well as BMP signal transduction. The non-opioid analgesics DCF and APAP distinctively modulate multiple reactions in the signaling network in both cell types: (1) enhance the presence of the negative regulator of IL-6 signal transduction SOCS3 particularly in PHH and (2) stabilize the BMP-ligand receptor interaction in the autocrine BMP-secretion loop in the hepatoma cell line HepG2, leading to increased hepcidin expression upon co-treatment with DCF or APAP.

Heterogeneous IL-6 responses determine the impact of DCF in PHH

In the context of liver cancer, both decreased and increased hepcidin levels have been reported, suggesting that hepcidin regulation is highly patient specific and may lead to heterogeneous and undesired responses to DCF and APAP treatment.[31]

First, we aimed to verify that the compounds distinctly affect IL-6-induced hepcidin expression through differences in activation of the SOCS3-mediated negative feedback loop in PHH and HepG2 cells. For these studies, we focused on the impact of DCF and analyzed the global proteome of HepG2 and PHH cells left untreated, treated with IL-6, or co-treated with IL-6/DCF for 6 h (Figure 6A). To assess SOCS3 activity, we quantified JAK1 protein levels, as SOCS3 binds to and promotes degradation of JAK1. In HepG2 cells, IL-6 induced only a transient SOCS3 expression, which was modestly enhanced by DCF co-treatment (Figure 2B). Accordingly, IL-6 treatment alone had no impact on JAK1 levels in these cells, while IL-6/DCF co-treatment led to a reduction in JAK1 abundance. In contrast, PHH show sustained IL-6 induced SOCS3 expression that was further amplified by DCF co-stimulation (Figure 5C). Correspondingly, JAK1 protein levels were reduced upon IL-6 treatment alone and even further reduced by co-treatment with IL-6 and DCF (Figure 6A). These results confirmed that DCF enhances the IL-6-induced negative feedback loop; however, the extent and impact are distinct between HepG2 cells and PHH, suggesting more pronounced SOCS3-mediated regulation in PHH.

To address the regulation of IL-6 responses in PHH from different patients and the impact on hepcidin expression, we analyzed the IL-6-induced expression dynamics of *SOCS3* (Figure 6B, left) and *HAMP* mRNA (Figure 6B, right) in PHH of four individual patients for up to 240 min. Interestingly, the extent of IL-6-induced *SOCS3* and *HAMP* mRNA expression was different in individual patients and negatively correlated, as for instance in patient 1, showing that the lowest IL-6-induced *SOCS3* mRNA expression corresponded to the highest IL-6-induced *HAMP* mRNA expression (Figure 6B). Furthermore, calculating the area under the curve confirmed a strong negative correlation between *SOCS3* and *HAMP* mRNA expression (Figure S4A, $r = -0.97$, p value = 0.033, $n = 4$). A comparison of *HAMP* mRNA expression in individual patients after 240 min of IL-6 stimulation in the absence or presence of DCF treatment

(B) Time-resolved and patient-specific IL-6-induced expression of SOCS3 and *HAMP* mRNA. mRNA amounts measured by quantitative real-time polymerase chain reaction were normalized to the housekeepers *HPRT* and *GAPDH*, $n = 1$.

(C) Bar plot showing the fold-change to 0 min in *HAMP* mRNA at 240 min of stimulation with IL-6 (black) or IL-6 and DCF (red) in individual patients. $n = 1$.

(D) Time-resolved fold changes in mRNA expression of *HAMP* mRNA compared with the untreated condition at 0 min following stimulation with different compounds. Shown are biological triplicates derived from patient 2. mRNA amounts measured by quantitative real-time polymerase chain reaction were normalized to the housekeepers *HPRT and GAPDH*. Shown are mean ± SD.

(E and F) Time-resolved predictions for *HAMP* mRNA expression in HepG2 cells using the integrative IL-6/STAT-BMP/SMAD model. Model trajectories, based on experimental data, for the impact of different parameters on *HAMP* mRNA expression in HepG2 cells treated with the indicated compounds or the simulated impact of a 4- or 16-fold parameter change are displayed.

(G and H) Model validation of the predicted impact of inhibition of BMPR activation on *HAMP* mRNA expression. HepG2 cells were treated with the indicated compounds as well as a dorsomorphin concentration resulting in a 4- or 16-fold inhibition of BMPR activation. *HAMP* mRNA expression was normalized to the housekeepers *HPRT*, *GAPDH*, and *TBP*. Different experiments were scaled to each other using a mixed-effect model within the *blotIt2* package in R. Error bars indicate the standard error of the mean, $n = 3$.

Table 1. Patient information

Patient	Age (years)	Gender	Diagnosis	Figure
1	46	male	colorectal cancer liver metastasis	Figures 1, 6A, S1, and S2
2	77	male	hepatocellular carcinoma	Figures 5E and 6B
3	67	male	cholangiocellular carcinoma	Figures 5E and 6B
4	39	male	esophageal carcinoma metastases	Figures 5E and 6B
5	51	female	leiomyosarcoma liver metastases	Figures 5E and 6B
6	48	female	colorectal cancer liver metastasis	Figure 5A
7	79	female	cholangiocellular carcinoma	Figure 5A
8	82	female	thyroid cancer	Figure 5A
9	64	male	cholangiocellular carcinoma	Figures 5A, 5E, and 6B
10	58	male	ileumcarcinoid liver metastasis	Figures 5A–5E and 6B
11	77	male	hepatocellular carcinoma	Figures 5A–5F, 6B, and 6D–6F
12	73	female	colorectal cancer liver metastasis	Figures 5A–5D, 5F, 6B, and 6D–6F
13	43	female	cholangiocellular carcinoma	Figures 5B–5D, 5F, 6B, 6D–6F, and S1
14	64	male	colorectal cancer liver metastasis	Figures 6A, 6D, and 6F

revealed that both the level of IL-6-induced *HAMP* mRNA and the impact of DCF were heterogeneous in the PHHs of individual patients (Figure 6C). In PHHs from patients with a $\log_{10}$ fold-change of *HAMP* mRNA smaller than 1.4, DCF had either no impact on *HAMP* mRNA or was inhibitory. Interestingly, in PHH from patient 1, which displayed the lowest SOCS3 induction, we observed a higher IL-6-mediated induction of *HAMP* mRNA and a slightly synergistic effect of DCF when combined with IL-6, reminiscent of the effects observed in HepG2. These results suggested that the extent of IL-6-induced SOCS3-mediated negative feedback loop is decisive for the inhibitory or synergistic effect of DCF on *HAMP* mRNA expression.

Different from the strongly synergistic impact of DCF on IL-6 induced *HAMP* mRNA expression observed in HepG2 cells, in most of the studied PHH a reduction of IL-6 induced *HAMP* mRNA expression upon co-stimulation with DCF was detected (Figure 6C). *HAMP* mRNA expression is regulated not only by IL-6 but also by BMPs. Since PHH lack the autocrine BMP-secretion loop present in HepG2 cells, we tested whether adding exogenous BMP could enhance *HAMP* mRNA induction in response to IL-6 and DCF. We exemplarily focused on PHH of patient 2 and tested the effect of IL-6/DCF/BMP2 on *HAMP* mRNA expression, both individually and in combination (Figure 6D). In these PHHs, treatment with IL-6 or BMP resulted in a similar, up to 14-fold, increase in the expression of *HAMP* mRNA, and co-treatment with BMP further increased the IL-6-mediated induction by 4-fold after 240 min, confirming synergistic effects of both factors in PHHs (Figure 6D). In line with Figure 6C, co-treatment with IL-6 and DCF resulted in a 4-fold reduction after 240 min of *HAMP* mRNA expression compared with IL-6-only treatment (Figure 6D). The synergistic effect between IL-6 and BMP2 on *HAMP* mRNA expression was lost when DCF was added, with a *HAMP* mRNA induction below IL-6 or BMP2 only treatments. These results suggested that in PHH of most patients, the DCF-mediated sustained SOCS3 expression dominates and prevents elevated levels of *HAMP* mRNA production upon IL-6, BMP and DCF co-treatment. In some PHHs, e.g., those from patient 1 that are characterized by lower SOCS3 levels, DCF could potentially amplify the IL-6- and BMP-induced *HAMP* mRNA expression similar to our observations in HepG2 cells leading to increased hepcidin production.

Here, we uncover that IL-6-induced activation of SOCS3 activity determines whether DCF has an inhibitory or activating effect on *HAMP* mRNA expression in PHH. We show that SOCS3 activity is highly patient specific and may be decisive for a patient's response to non-opioid analgesics.

Identification of inhibition of BMPR activity as target to decrease *HAMP* mRNA levels in hepatoma cells

Exceedingly high levels of hepcidin in the blood are pathogenic leading to functional iron deficiency and intensified anemia in patients.[32] Since patients, especially the ones suffering from chronic diseases such as cancer, frequently take non-opioid analgesics, our results indicate that this treatment may have undesired side effects. To counter act those, we utilized our mathematical pathway model to propose intervention strategies. First, we performed model simulations to investigate, which intervention would reduce the observed increased expression of *HAMP* mRNA expression in HepG2 cells co-treated with IL-6 and DCF or APAP. Based on our results, we selected previously identified parameters primarily affected by DCF or APAP treatment and calculated how much impact an increase in the corresponding parameter would have on *HAMP* mRNA expression. We focused our evaluations on four different interventions: (1) enhancement of the SOCS3 protein production; (2) inhibition of the drug-mediated *HAMP* mRNA degradation; (3) inhibition of IL-6 receptor activation, and (4) inhibition of BMPR activation. The simulations predicted that even a 16-fold increase in SOCS3 protein production or inhibition of IL-6 receptor activation would only slightly reduce predicted *HAMP* mRNA levels in IL-6- and DCF- (Figure 6E, left) or APAP-co-treated HepG2 cells (Figure 6F, left). Increasing the DCF-mediated (Figure 6A, top right) or APAP-mediated (Figure 6F, top right) inhibition of *HAMP* mRNA degradation could potentially reduce predicted *HAMP* mRNA levels, but not to steady-state levels of IL-6 treated samples. The inhibition of BMPR activation was predicted to have the strongest impact on *HAMP* mRNA expression upon co-stimulation with IL-6 and

DCF (Figure 6E, bottom right) or APAP (Figure 6F, bottom right). A 4-fold increase in this parameter was predicted to already reduce the expression of *HAMP* mRNA levels to levels comparable to IL-6 stimulation alone.

To experimentally validate this model-based hypothesis, we first determined suitable concentrations of dorsomorphin to achieve a 4- and 16-fold reduction of SMAD1/5/8 phosphorylation in HepG2 cells upon IL-6 and DCF or APAP co-stimulation: in the presence of DCF, 1.67 μM dorsomorphin (4-fold reduction) and 3.35 μM dorsomorphin (for 16-fold reduction) were required, whereas for APAP 1.14 and 2.28 μM of dorsomorphin, respectively, were sufficient (Figure S4B). Subsequently, we evaluated the effect of the BMPR inhibition on *HAMP* mRNA gene expression. In line with the model predictions, the treatment with a respective DCF (Figure 6G, orange line) or APAP concentration (Figure 6H, light green line) to achieve a 4-fold parameter reduction led to a significant reduction of *HAMP* mRNA expression. Increasing the dorsomorphin concentrations to induce a 16-fold increase in inhibition had no further effect on DCF-induced *HAMP* mRNA expression (Figure 6G yellow line) but slightly further decreased APAP-induced gene expression (Figure 6H, lime green line). Furthermore, as predicted by the mathematical model (Figures 6E and 6F, gray lines in bottom right), the experimental data also showed the reduction of *HAMP* mRNA by dorsomorphin in HepG2 cells treated with IL-6 alone, further supporting a crosstalk between the IL-6 and BMP signaling pathways.

In conclusion, utilizing an integrative mathematical modeling approach, we predict that the non-opioid analgesics DCF and APAP upregulate autocrine BMP signaling in hepatoma cells and, as a consequence, amplify the expression of systemically acting iron regulator hepcidin, which can be counteracted by BMPR inhibition.

DISCUSSION

Non-opioid analgesics such as DCF and APAP are widely used for pain management, including pain in cancer patients. Common knowledge on their mode of action has been that DCF and APAP inhibit the cyclooxygenases COX-1 and -2,[3,33] which convert arachidonic acid to prostaglandins, leading to increased IL-6 secretion and enhanced immune responses. In this study, we show that DCF and APAP can directly modulate IL-6 and BMP signal transduction altering the regulation of iron metabolism in a patient- and cell-type-specific manner. We observed that upon IL6 and DCF co-treatment the expression of the key regulator of iron metabolism hepcidin encoded by *HAMP* mRNA is amplified in the hepatoma cell line HepG2 and reduced in the majority of PHH. In some patients an enhancement *HAMP* mRNA expression is detected, pointing to inter-patient heterogeneity in the regulation of HAMP mRNA expression and the impact of DCF. In liver cancer cells, such as HepG2 cells, model-based simulations and experimental validation identify inference at the BMPR level as most promising to prevent amplified hepcidin expression due to IL-6 and DCF co-exposure and thus potential undesired side effects. This observation is of particular relevance for cancer patients because they regularly suffer from iron-deficiency-caused anemia due to increased hepcidin levels.[34,35]

Interaction of IL-6 and BMP2 signal transduction pathways

One observation of our study is that DCF and APAP amplify the IL-6-mediated expression of *HAMP* mRNA in liver cancer cells through autocrine BMP signal transduction and down regulation of the negative feedback regulator SMAD6. This is supported by the finding that BMP and IL-6 ligands synergistically enhance the activity of the *HAMP* mRNA promotor and thus increase *HAMP* mRNA expression in HepG2 cells.[11,29] Further, Mleczko and colleagues reported that DCF exposure in the hepatoma cell line Huh7 for 24 h enhances *HAMP* mRNA expression.[17] Our studies provide a potential explanation for these observations and demonstrate that this is an early effect, already present at 1 h after DCF or APAP exposure. This rapid onset indicates that the effect is likely not dependent on a conversion to bio-reactive compounds, which have previously been considered essential, especially for APAP activity.[5] Instead, it may result from direct interaction with signal transduction components such as the stabilization of the BMP ligand-receptor interaction.

Impact on iron metabolism

We provide evidence that through the impact on inflammatory signal transduction DCF and APAP modulate the expression of hepcidin, a systemic regulator of iron metabolism, and thus could affect multiple processes in the body. To link cellular scale insights to an organ scale regulatory network of iron metabolism, in a previous study, Lopes et al. developed a mathematical model describing the dynamics of the iron flux between organs in mice.[36] Likewise, a whole-body model of iron homeostasis in the mouse describes hepcidin expression as well as iron fluxes in liver, spleen, serum, red blood cells, and other organs.[37] Interestingly, in support of our study of the synergistic effect of IL-6 and BMP signal transduction in amplifying *HAMP* mRNA expression, the authors uncovered that it was necessary to consider regulatory mechanisms of pro-inflammatory signal transduction to fully explain serum iron levels. Their final model was capable of describing the massive induction of *HAMP* mRNA expression upon an iron-rich diet, which activates the BMP/SMAD pathway and upon LPS injection triggering the secretion of inflammatory factors such as IL-6. The model-predicted iron accumulation in liver and spleen in these mice, which was experimentally confirmed. Furthermore, a mathematical model of cellular iron metabolism that was based on clinical data was able to describe *HAMP* mRNA expression in relation to liver and plasma iron levels and the concentrations of proteins such as ferroportin and ferritin[38] but lacked the input from inflammatory factors. Therefore, it could be of interest to integrate our mechanistic mathematical model in one of these existing models to explore the impact of APAP and DCF also at a larger scale and to investigate the impact of drug-induced iron overload at the organism scale.

Differential reactions of tumor-derived and non-cancerous hepatocytes

In the context of cancer, research has primarily focused on the hepatotoxic effects of chemotherapeutic agents,[39] whereas the potential side effects of commonly used pain medications have so far not been considered. Cancer cells substantially differ in their response to stimuli through signal transduction networks

compared with non-tumor cells.[40] Studying the cellular responses in different cellular systems (PHH and hepatoma cell line HepG2) revealed that PHH respond differently to co-stimulation of IL-6 and DCF/APAP than HepG2 cells. Most patient-derived, but non-cancerous PHH, did not show a synergistic effect on *HAMP* mRNA expression when co-stimulated with IL-6 and DCF/APAP. Absence of the autocrine BMP signaling loop alone, uncovered in the hepatoma cells, could not account for this discrepancy, as exogenous supplementation of BMP2 failed to establish the amplified *HAMP* mRNA expression dynamics detected in HepG2 cells.

The sustained Il-6-induced *SOCS3* expression in PHHs was an additional distinguishing factor compared with the transient *SOCS3* induction observed in HepG2 cells. This observation suggests the presence of a more robust activation of the SOCS3-mediated negative feedback loop targeting the IL-6 receptor in PHH.[7] This hypothesis was supported by our proteome analysis showing that in response to IL-6 stimulation, the abundance of JAK1, due to its association with the IL-6 receptor serving as proxy, was significantly decreased in PHHs but unchanged in JAK1 in HepG2 cells. The observed inter-patient heterogeneity in the strength of IL-6 induced feedback regulation in individual patients and the strong negative correlation with HAMP mRNA expression underscores the direct impact of SOCS3 on the downregulation of IL-6-induced signal transduction. SOCS3 binds to the IL-6 receptor and promotes its degradation,[41] along with the receptor-bound kinase JAK1, ultimately reducing the expression of *HAMP* mRNA, the key regulator of iron homeostasis. Notably, PHH derived from the patient with the weakest *SOCS3* response exhibited an additive effect on *HAMP* mRNA expression following IL-6 and DCF co-treatment, similar to the observations in the hepatoma cell line HepG2. A potential molecular explanation for the observed heterogeneity and the cell-context-specific differences could be the methylation status of the *SOCS3* promoter. In a previous study, using dynamic pathway modeling, we identified SOCS3 activity as the most distinct parameter between primary and cancer cells and experimentally confirmed partial *SOCS3* promoter methylation.[24] Furthermore, *SOCS3* methylation has been reported to be associated with poor overall survival in HCC patients.[42] Investigating the relationship between *SOCS3* methylation and hepatocyte responsiveness to IL-6 and DCF or APAP may provide additional insights in the consequences of non-opioid analgesics.[42]

Inter-patient variability and clinical implications

Our findings highlight the inter-patient variability of IL-6-induced responses in the liver with a tight link to the regulation of iron homeostasis and point to a risk of using DCF or APAP in patients with low SOCS3 responsiveness. In such individuals, the non-opioid analgesics could result in excessive *HAMP* mRNA expression, contributing to or exacerbating anemia.[43] Although solid tumors such as liver cancer occur—at least initially—locally, increased hepcidin levels act systemically and thus could foster anemia. These insights emphasize the need for personalized approaches in pain management, especially in vulnerable populations such as cancer patients who are already at risk for iron-restricted anemia. Interestingly, in a recent study, daily low dose of aspirin, another broadly used non-opioid analgesic, was linked to an increased incidence of anemia in elderly people.[44] Our findings imply that the analgesic treatment with DCF and APAP could aggravate anemia by further lowering serum iron via BMP-induced hepcidin overexpression through the stabilization of ligand-receptor interaction. Predictions with our integrative mathematical model of IL-6 and BMP signal transduction capturing the impact of DCF and APAP allowed to pinpoint relevant targets in the complex network. We showed that the partial inhibition of BMP-ligand-induced receptor activation in the hepatoma cell line HepG2 efficiently reduced excessive hepcidin production but did not affect the basal hepcidin expression in response to IL-6 treatment only. Clinically, this could be realized with compounds targeting the BMPR such as dorsomorphin derivatives[20,21] and could potentially contribute to preventing anemia in patients with liver cancer.

Limitations of the study

In this study, we demonstrated that both DCF and APAP modulate IL-6-mediated signal transduction in the hepatoma cell line HepG2 and in PHHs. In addition, both compounds trigger the activation of BMP signal transduction in hepatoma cells and thereby further amplify the induction of the central iron regulator hepcidin. These results underline that although it is possible to utilize the hepatoma cell line HepG2 as model system to study drug effects *in vitro*, some of the observed effects might not apply directly to patients. Moreover, although PHH provide a more physiologically relevant model, they still represent a simplified system and may not fully mirror the complexity of liver function *in vivo*. Therefore, caution is warranted when extrapolating these *in vitro* findings to whole-organ or patient-level outcomes.

RESOURCE AVAILABILITY

Lead contact

Further information and requests for resources and reagents should be directed to and will be fulfilled by the lead contact, Ursula Klingmüller (u.klingmueller@dkfz.de).

Materials availability

This study did not generate new unique reagents.

Data and code availability

The MS proteomics data have been deposited to the ProteomeXchange Consortium via the PRIDE[45] partner repository. The HepG2 proteome data were deposited with the dataset identifier PRIDE: PXD054756. The PHH proteome data were deposited with the dataset identifier PRIDE: PXD054759.

The integrative HepG2 model and the PHH model are provided as SBML model files (HepG2_model.xml and PHH_model.xml). The models were also deposited in BioModels (https://www.ebi.ac.uk/biomodels/)[46] and assigned to the identifiers MODEL2503270001 (HepG2) and MODEL2503270002 (PHH).

All modeling scripts and results are available from the D2D GitHub repository at this link. An archived version of the repository is available on Zenodo and can be cited using the following DOI: https://doi.org/10.5281/zenodo.16411068.

Any additional information required to reanalyze the data reported in this paper is available from the lead contact upon request.

ACKNOWLEDGMENTS

We thank Yannik Dieter, Franziska Gödtel, Marie Buck-Wiese, and Lena Postawa for excellent technical assistance. We acknowledge funding from the German Federal Ministry of Research, Technology and Space (BMFTR) within the Liver Systems Medicine network (LiSyM, 031L0042and 031L0048), the

LiSyM-Cancer network SMART-NAFLD (031L0256A, 031L0313A, 031L 0256C, and 031L0313C), and C-TIP-HCC (031L0257C and 031L0314C); the e:Bio collaborative research projects "Multi-Scale Modeling of Drug-Induced Liver Injury" (MS_DILI, 031L0074A and 031L0074B); the EraSysAPP consortium IMOMESIC (031A604A, 031A604B, and 031A604C); and The German Center for Lung Research (DZL, 82DZL004A4). We also acknowledge funding by HORIZON EUROPE of the European Research Council within the network ARTEMIS (101136299) and from the Deutsche Forschungsgemeinschaft (DFG) within Germany's Excellence Strategy (CIBSS – EXC-2189 – Project ID 390939984), the INST 35/1134-1 FUGG, the TRR179 (272983813), and FerrOs – FOR-5146 (436298031). We further acknowledge funding from the state of Baden-Württemberg through bwHPC.

AUTHOR CONTRIBUTIONS

A.Z., J.V., C.M., P.K., M.S., J.T., and U.K. were responsible for study conception and design. A.Z., A.V., C.M., P.K., B.H., A.H., T.M., and E.H. acquired the data. S.W., K.H., G.S., A.S., M.K., E.G.-B., C.K., C.M., D.S., and G.D. provided primary human hepatocytes. A.Z., C.M., P.K., T.M., J.V., A.V., S.B.d.L., and N. L. performed the analysis and interpretation of data. A.Z., C.M., P.K., J.V., A.V., M.S., M.U.M., and U.K. drafted the manuscript and all authors critically revised the manuscript.

DECLARATION OF INTERESTS

The authors declare no competing interests.

STAR★METHODS

Detailed methods are provided in the online version of this paper and include the following:

- KEY RESOURCES TABLE
- EXPERIMENTAL MODEL AND SUBJECT DETAILS
  - Isolation of primary human hepatocytes
  - Cell culture
  - Drug, inhibitor and cytokine treatments
  - Cell lysis and protein amount determination
  - Preparation of cell lysate samples for mass spectrometry analysis
  - Cell lysis for quantitative immunoblotting
- METHOD DETAILS
  - Quantitative immunoblotting
  - Quantification of target gene expression by quantitative real-time PCR (qRT-PCR)
  - Bead-based immunoassay and ELISA
  - Global Mass Spectrometry (MS)
  - Database search and data analysis
- QUANTIFICATION AND STATISTICAL ANALYSIS
  - Statistical analysis of DIA data
  - Mathematical modeling
  - Plotting
  - L_1-regularization

SUPPLEMENTAL INFORMATION

Supplemental information can be found online at https://doi.org/10.1016/j.cels.2025.101431.

Received: August 27, 2024
Revised: June 6, 2025
Accepted: October 9, 2025
Published: November 10, 2025

REFERENCES

1. Ventafridda, V., Saita, L., Ripamonti, C., and De Conno, F. (1985). WHO guidelines for the use of analgesics in cancer pain. Int. J. Tissue React. *7*, 93–96.
2. Altman, R., Bosch, B., Brune, K., Patrignani, P., and Young, C. (2015). Advances in NSAID development: evolution of diclofenac products using pharmaceutical technology. Drugs *75*, 859–877. https://doi.org/10.1007/s40265-015-0392-z.
3. Sallmann, A.R. (1986). The history of diclofenac. Am. J. Med. *80*, 29–33. https://doi.org/10.1016/0002-9343(86)90076-8.
4. Ganz, T., and Nemeth, E. (2012). Hepcidin and iron homeostasis. Biochim. Biophys. Acta *1823*, 1434–1443. https://doi.org/10.1016/j.bbamcr.2012.01.014.
5. Ghanem, C.I., Pérez, M.J., Manautou, J.E., and Mottino, A.D. (2016). Acetaminophen from liver to brain: New insights into drug pharmacological action and toxicity. Pharmacol. Res. *109*, 119–131. https://doi.org/10.1016/j.phrs.2016.02.020.
6. Hinson, R.M., Williams, J.A., and Shacter, E. (1996). Elevated interleukin 6 is induced by prostaglandin E2 in a murine model of inflammation: possible role of cyclooxygenase-2. Proc. Natl. Acad. Sci. USA *93*, 4885–4890. https://doi.org/10.1073/pnas.93.10.4885.
7. Schaper, F., and Rose-John, S. (2015). Interleukin-6: Biology, signaling and strategies of blockade. Cytokine Growth Factor Rev. *26*, 475–487. https://doi.org/10.1016/j.cytogfr.2015.07.004.
8. Castell, J.V., Gómez-Lechón, M.J., David, M., Fabra, R., Trullenque, R., and Heinrich, P.C. (1990). Acute-phase response of human hepatocytes: regulation of acute-phase protein synthesis by interleukin-6. Hepatology *12*, 1179–1186. https://doi.org/10.1002/hep.1840120517.
9. Sobotta, S., Raue, A., Huang, X., Vanlier, J., Jünger, A., Bohl, S., Albrecht, U., Hahnel, M.J., Wolf, S., Mueller, N.S., et al. (2017). Model Based Targeting of IL-6-Induced Inflammatory Responses in Cultured Primary Hepatocytes to Improve Application of the JAK Inhibitor Ruxolitinib. Front. Physiol. *8*, 775. https://doi.org/10.3389/fphys.2017.00775.
10. Nemeth, E., Rivera, S., Gabayan, V., Keller, C., Taudorf, S., Pedersen, B. K., and Ganz, T. (2004). IL-6 mediates hypoferremia of inflammation by inducing the synthesis of the iron regulatory hormone hepcidin. J. Clin. Invest. *113*, 1271–1276. https://doi.org/10.1172/JCI20945.
11. Casanovas, G., Banerji, A., d'Alessio, F., Muckenthaler, M.U., and Legewie, S. (2014). A multi-scale model of hepcidin promoter regulation reveals factors controlling systemic iron homeostasis. PLoS Comput. Biol. *10*, e1003421. https://doi.org/10.1371/journal.pcbi.1003421.
12. Breitkopf-Heinlein, K., Meyer, C., König, C., Gaitantzi, H., Addante, A., Thomas, M., Wiercinska, E., Cai, C., Li, Q., Wan, F., et al. (2017). BMP-9 interferes with liver regeneration and promotes liver fibrosis. Gut *66*, 939–954. https://doi.org/10.1136/gutjnl-2016-313314.
13. Xiao, X., Alfaro-Magallanes, V.M., and Babitt, J.L. (2020). Bone morphogenic proteins in iron homeostasis. Bone *138*, 115495. https://doi.org/10.1016/j.bone.2020.115495.
14. von Bubnoff, A., and Cho, K.W. (2001). Intracellular BMP signaling regulation in vertebrates: pathway or network? Dev. Biol. *239*, 1–14. https://doi.org/10.1006/dbio.2001.0388.
15. Lasorella, A., Benezra, R., and Iavarone, A. (2014). The ID proteins: master regulators of cancer stem cells and tumour aggressiveness. Nat. Rev. Cancer *14*, 77–91. https://doi.org/10.1038/nrc3638.
16. Lai, D., Teng, F., Hammad, S., Werle, J., Maas, T., Teufel, A., Muckenthaler, M.U., Dooley, S., and Vujić Spasić, M. (2018). Hepatic Smad7 overexpression causes severe iron overload in mice. Blood *131*, 581–585. https://doi.org/10.1182/blood-2017-07-796797.
17. Mleczko-Sanecka, K., da Silva, A.R., Call, D., Neves, J., Schmeer, N., Damm, G., Seehofer, D., and Muckenthaler, M.U. (2017). Imatinib and spironolactone suppress hepcidin expression. Haematologica *102*, 1173–1184. https://doi.org/10.3324/haematol.2016.162917.
18. Wang, R.N., Green, J., Wang, Z., Deng, Y., Qiao, M., Peabody, M., Zhang, Q., Ye, J., Yan, Z., Denduluri, S., et al. (2014). Bone Morphogenetic Protein (BMP) signaling in development and human diseases. Genes Dis. *1*, 87–105. https://doi.org/10.1016/j.gendis.2014.07.005.

19. Walsh, D.W., Godson, C., Brazil, D.P., and Martin, F. (2010). Extracellular BMP-antagonist regulation in development and disease: tied up in knots. Trends Cell Biol. *20*, 244–256. https://doi.org/10.1016/j.tcb.2010.01.008.

20. Yu, P.B., Hong, C.C., Sachidanandan, C., Babitt, J.L., Deng, D.Y., Hoyng, S.A., Lin, H.Y., Bloch, K.D., and Peterson, R.T. (2008). Dorsomorphin inhibits BMP signals required for embryogenesis and iron metabolism. Nat. Chem. Biol. *4*, 33–41. https://doi.org/10.1038/nchembio.2007.54.

21. Sison-Young, R.L., Lauschke, V.M., Johann, E., Alexandre, E., Antherieu, S., Aerts, H., Gerets, H.H.J., Labbe, G., Hoët, D., Dorau, M., et al. (2017). A multicenter assessment of single-cell models aligned to standard measures of cell health for prediction of acute hepatotoxicity. Arch. Toxicol. *91*, 1385–1400. https://doi.org/10.1007/s00204-016-1745-4.

22. Wiśniewski, J.R., Vildhede, A., Norén, A., and Artursson, P. (2016). In-depth quantitative analysis and comparison of the human hepatocyte and hepatoma cell line HepG2 proteomes. J. Proteomics *136*, 234–247. https://doi.org/10.1016/j.jprot.2016.01.016.

23. D'Alessandro, L.A., Klingmüller, U., and Schilling, M. (2022). Deciphering signal transduction networks in the liver by mechanistic mathematical modelling. Biochem. J. *479*, 1361–1374. https://doi.org/10.1042/BCJ20210548.

24. Merkle, R., Steiert, B., Salopiata, F., Depner, S., Raue, A., Iwamoto, N., Schelker, M., Hass, H., Wäsch, M., Böhm, M.E., et al. (2016). Identification of Cell Type-Specific Differences in Erythropoietin Receptor Signaling in Primary Erythroid and Lung Cancer Cells. PLoS Comput. Biol. *12*, e1005049. https://doi.org/10.1371/journal.pcbi.1005049.

25. Krämer, A., Green, J., Pollard, J., Jr., and Tugendreich, S. (2014). Causal analysis approaches in Ingenuity Pathway Analysis. Bioinformatics *30*, 523–530. https://doi.org/10.1093/bioinformatics/btt703.

26. Oppelt, A., Kaschek, D., Huppelschoten, S., Sison-Young, R., Zhang, F., Buck-Wiese, M., Herrmann, F., Malkusch, S., Krüger, C.L., Meub, M., et al. (2018). Model-based identification of TNFα-induced IKKβ-mediated and IκBα-mediated regulation of NFκB signal transduction as a tool to quantify the impact of drug-induced liver injury compounds. NPJ Syst. Biol. Appl. *4*, 23. https://doi.org/10.1038/s41540-018-0058-z.

27. Gerhartz, C., Dittrich, E., Stoyan, T., Rose-John, S., Yasukawa, K., Heinrich, P.C., and Graeve, L. (1994). Biosynthesis and half-life of the interleukin-6 receptor and its signal transducer gp130. Eur. J. Biochem. *223*, 265–274. https://doi.org/10.1111/j.1432-1033.1994.tb18991.x.

28. Raue, A., Kreutz, C., Maiwald, T., Bachmann, J., Schilling, M., Klingmüller, U., and Timmer, J. (2009). Structural and practical identifiability analysis of partially observed dynamical models by exploiting the profile likelihood. Bioinformatics *25*, 1923–1929. https://doi.org/10.1093/bioinformatics/btp358.

29. Steinbicker, A.U., Sachidanandan, C., Vonner, A.J., Yusuf, R.Z., Deng, D.Y., Lai, C.S., Rauwerdink, K.M., Winn, J.C., Saez, B., Cook, C.M., et al. (2011). Inhibition of bone morphogenetic protein signaling attenuates anemia associated with inflammation. Blood *117*, 4915–4923. https://doi.org/10.1182/blood-2010-10-313064.

30. Raue, A., Schilling, M., Bachmann, J., Matteson, A., Schelker, M., Kaschek, D., Hug, S., Kreutz, C., Harms, B.D., Theis, F.J., et al. (2013). Lessons learned from quantitative dynamical modeling in systems biology. PLoS One *8*, e74335. https://doi.org/10.1371/journal.pone.0074335.

31. Joachim, J.H., and Mehta, K.J. (2022). Hepcidin in hepatocellular carcinoma. Br. J. Cancer *127*, 185–192. https://doi.org/10.1038/s41416-022-01753-2.

32. Ganz, T. (2013). Systemic iron homeostasis. Physiol. Rev. *93*, 1721–1741. https://doi.org/10.1152/physrev.00008.2013.

33. Flower, R.J., and Vane, J.R. (1972). Inhibition of prostaglandin synthetase in brain explains the anti-pyretic activity of paracetamol (4-acetamidophenol). Nature *240*, 410–411. https://doi.org/10.1038/240410a0.

34. Birgegård, G., Aapro, M.S., Bokemeyer, C., Dicato, M., Drings, P., Hornedo, J., Krzakowski, M., Ludwig, H., Pecorelli, S., Schmoll, H., et al. (2005). Cancer-related anemia: pathogenesis, prevalence and treatment. Oncology *68*, 3–11. https://doi.org/10.1159/000083128.

35. Nemeth, E., and Ganz, T. (2023). Hepcidin and Iron in Health and Disease. Annu. Rev. Med. *74*, 261–277. https://doi.org/10.1146/annurev-med-043021-032816.

36. Lopes, T.J.S., Luganskaja, T., Vujić Spasić, M., Hentze, M.W., Muckenthaler, M.U., Schümann, K., and Reich, J.G. (2010). Systems analysis of iron metabolism: the network of iron pools and fluxes. BMC Syst. Biol. *4*, 112. https://doi.org/10.1186/1752-0509-4-112.

37. Enculescu, M., Metzendorf, C., Sparla, R., Hahnel, M., Bode, J., Muckenthaler, M.U., and Legewie, S. (2017). Modelling Systemic Iron Regulation during Dietary Iron Overload and Acute Inflammation: Role of Hepcidin-Independent Mechanisms. PLoS Comput. Biol. *13*, e1005322. https://doi.org/10.1371/journal.pcbi.1005322.

38. Mitchell, S., and Mendes, P. (2013). A computational model of liver iron metabolism. PLoS Comput. Biol. *9*, e1003299. https://doi.org/10.1371/journal.pcbi.1003299.

39. Vincenzi, B., Armento, G., Spalato Ceruso, M., Catania, G., Leakos, M., Santini, D., Minotti, G., and Tonini, G. (2016). Drug-induced hepatotoxicity in cancer patients - implication for treatment. Expert Opin. Drug Saf. *15*, 1219–1238. https://doi.org/10.1080/14740338.2016.1194824.

40. Sever, R., and Brugge, J.S. (2015). Signal transduction in cancer. Cold Spring Harb. Perspect. Med. *5*, a006098. https://doi.org/10.1101/cshperspect.a006098.

41. Kershaw, N.J., Laktyushin, A., Nicola, N.A., and Babon, J.J. (2014). Reconstruction of an active SOCS3-based E3 ubiquitin ligase complex in vitro: identification of the active components and JAK2 and gp130 as substrates. Growth Factors *32*, 1–10. https://doi.org/10.3109/08977194.2013.877005.

42. Jiang, B.G., Wang, N., Huang, J., Yang, Y., Sun, L.L., Pan, Z.Y., and Zhou, W.P. (2017). Tumor SOCS3 methylation status predicts the treatment response to TACE and prognosis in HCC patients. Oncotarget *8*, 28621–28627. https://doi.org/10.18632/oncotarget.16157.

43. Gaspar, B.L., Sharma, P., and Das, R. (2015). Anemia in malignancies: pathogenetic and diagnostic considerations. Hematology *20*, 18–25. https://doi.org/10.1179/1607845414Y.0000000161.

44. McQuilten, Z.K., Thao, L.T.P., Pasricha, S.R., Artz, A.S., Bailey, M., Chan, A.T., Cohen, H.J., Lockery, J.E., Murray, A.M., Nelson, M.R., et al. (2023). Effect of Low-Dose Aspirin Versus Placebo on Incidence of Anemia in the Elderly: A Secondary Analysis of the Aspirin in Reducing Events in the Elderly Trial. Ann. Intern. Med. *176*, 913–921. https://doi.org/10.7326/M23-0675.

45. Perez-Riverol, Y., Bai, J., Bandla, C., García-Seisdedos, D., Hewapathirana, S., Kamatchinathan, S., Kundu, D.J., Prakash, A., Frericks-Zipper, A., Eisenacher, M., et al. (2022). The PRIDE database resources in 2022: a hub for mass spectrometry-based proteomics evidences. Nucleic Acids Res. *50*, D543–D552. https://doi.org/10.1093/nar/gkab1038.

46. Chelliah, V., Juty, N., Ajmera, I., Ali, R., Dumousseau, M., Glont, M., Hucka, M., Jalowicki, G., Keating, S., Knight-Schrijver, V., et al. (2015). BioModels: ten-year anniversary. Nucleic Acids Res. *43*, D542–D548. https://doi.org/10.1093/nar/gku1181.

47. Ritchie, M.E., Phipson, B., Wu, D., Hu, Y., Law, C.W., Shi, W., and Smyth, G.K. (2015). limma powers differential expression analyses for RNA-sequencing and microarray studies. Nucleic Acids Res. *43*, e47. https://doi.org/10.1093/nar/gkv007.

48. Heming, S., Hansen, P., Vlasov, A., Schwörer, F., Schaumann, S., Frolovaitė, P., Lehmann, W.D., Timmer, J., Schilling, M., Helm, B., et al. (2022). MSPypeline: a python package for streamlined data analysis of mass spectrometry-based proteomics. Bioinform. Adv. *2*, vbac004. https://doi.org/10.1093/bioadv/vbac004.

49. Kemmer, S., Bang, S., Rosenblatt, M., Timmer, J., and Kaschek, D. (2022). BlotIt-Optimal alignment of Western blot and qPCR experiments. PLoS One *17*, e0264295. https://doi.org/10.1371/journal.pone.0264295.

50. Burbano de Lara, S., Kemmer, S., Biermayer, I., Feiler, S., Vlasov, A., D'Alessandro, L.A., Helm, B., Mölders, C., Dieter, Y., Ghallab, A., et al. (2024). Basal MET phosphorylation is an indicator of hepatocyte

dysregulation in liver disease. Mol. Syst. Biol. *20*, 187–216. https://doi.org/10.1038/s44320-023-00007-4.

51. Müller, T., Kalxdorf, M., Longuespée, R., Kazdal, D.N., Stenzinger, A., and Krijgsveld, J. (2020). Automated sample preparation with SP3 for low-input clinical proteomics. Mol. Syst. Biol. *16*, e9111. https://doi.org/10.15252/msb.20199111.
52. Schilling, M., Maiwald, T., Bohl, S., Kollmann, M., Kreutz, C., Timmer, J., and Klingmüller, U. (2005). Computational processing and error reduction strategies for standardized quantitative data in biological networks. FEBS J. *272*, 6400–6411. https://doi.org/10.1111/j.1742-4658.2005.05037.x.
53. Raue, A., Steiert, B., Schelker, M., Kreutz, C., Maiwald, T., Hass, H., Vanlier, J., Tönsing, C., Adlung, L., Engesser, R., et al. (2015). Data2Dynamics: a modeling environment tailored to parameter estimation in dynamical systems. Bioinformatics *31*, 3558–3560. https://doi.org/10.1093/bioinformatics/btv405.
54. MacDonald, N. (1976). Time delay in simple chemostat models. Biotechnol. Bioeng. *18*, 805–812. https://doi.org/10.1002/bit.260180604.
55. Maiwald, T., Hass, H., Steiert, B., Vanlier, J., Engesser, R., Raue, A., Kipkeew, F., Bock, H.H., Kaschek, D., Kreutz, C., et al. (2016). Driving the Model to Its Limit: Profile Likelihood Based Model Reduction. PLoS One *11*, e0162366. https://doi.org/10.1371/journal.pone.0162366.
56. Steiert, B., Timmer, J., and Kreutz, C. (2016). L1 regularization facilitates detection of cell type-specific parameters in dynamical systems. Bioinformatics *32*, i718–i726. https://doi.org/10.1093/bioinformatics/btw461.

STAR★METHODS

KEY RESOURCES TABLE

REAGENT or RESOURCE	SOURCE	IDENTIFIER
Antibodies		
pSmad1/5/8	MaineHealth	Cat#Vli31-5 RRID:AB_10013240
Smad1	Cell Signaling Technology	Cat#9743; RRID:AB_2107780
pSTAT3 (Y705)	Cell Signaling Technology	Cat# 9138 RRID:AB_331262
STAT3alpha	Cell Signaling Technology	Cat#8768 RRID:AB_2722529
SOCS3 (clone 1B2, for IP)	Life Technologies GmbH	Cat#377200 RRID:AB_431465
SOCS3	Abcam	Cat#ab16030; RRID: AB_443287
gp130 (C20) (for IP)	Santa Cruz Biotechnology	Cat#sc-655 RRID:AB_631590
gp130 (for IB)	Upstate Millipore	Cat#06-291; RRID: AB_310091
b-Actin	Santa Cruz Biotechnology	Cat# sc-47778 RRID:AB_626632
HRP-coupled goat anti-rabbit IgG	Jackson ImmunoResearch Labs	Cat# 111-035-144; RRID:AB_2307391
HRP-coupled goat anti-mouse IgG	Jackson ImmunoResearch Labs	Cat# 115-035-146 RRID:AB_2307392
Chemicals, peptides, and recombinant proteins		
Actinomycin D	Sigma Aldrich	Cat#A1410
Dorsomorphin	Cayman Chemicals	Cat#11967
LDN-193189	TargetMol	Cat#T1935
recombinant human BMP-2	Novus Biologicals	Cat#NBP2-34928
recombinant human IL-6	R&D Systems	Cat#206-IL
Diclofenac sodium salt	Sigma Aldrich	Cat#D6899
Acetaminophen	Sigma Aldrich	Cat#A7085
BSA	Sigma Aldrich	Cat#A7906-500g
EDTA	Applichem	Cat#A3145,0500
DPBS	PAN Biotech	Cat#P04-36500
Williams medium E, without L-glutamine and phenol red	Sigma Aldrich	Cat#W1878
Fetal bovine serum	Thermo Fisher Scientific	Cat#10082147
Dexamethasone	Thermo Fisher Scientific	Cat#A13449
Insulin-Transferrin-Selen (ITS-G)	Thermo Fisher Scientific	Cat#41400045
L-Glutamine	Thermo Fisher Scientific	Cat#25030081
Penicillin/Streptinomycin	Thermo Fisher Scientific	Cat#15140122
Dulbecco's modified Eagle medium	Thermo Fisher Scientific	Cat#31053028
Sodium Pyruvate	Thermo Fisher Scientific	Cat#11360070
SpeedBeads magnetic carboxylate modified particles	Cytiva	Cat#65152105050250
SpeedBeads magnetic carboxylate modified particles	Cytiva	Cat#45152105050250
Critical commercial assays		
NucleoSpin RNA isolation kit	Macherey Nagel	Cat#740955.50
High-Capacity cDNA Reverse Transcription Kit	Applied Biosystems	Cat#4368814
Human Luminex® Discovery Assay	R&D Systems	Cat#LXSAHM
BMP-2 Quantikine ELISA Kit	R&D Systems	Cat#DBP200
Pierce™ BCA Protein Assay Kit	Thermo Scientific	Cat#23225
Deposited data		
Proteomes of HepG2 cells	This paper	PXD054756
Proteomes of primary human hepatocytes	This paper	PXD054759

(*Continued on next page*)

Continued

REAGENT or RESOURCE	SOURCE	IDENTIFIER
Experimental models: Cell lines		
Hep-G2	ATCC	RRID:CVCL_0027
Oligonucleotides		
hSOCS3 qPCR primer 1 5'-AGACTTCGATTCGGGACCA-3'	This paper	Roche UPL: #36
hSOCS3 qPCR primer 2 5'- AACTTGCTGTGGGTGACCA-3'	This paper	Roche UPL: #36
hA2M qPCR primer 1 5'-TGTGAGAAATTCAGTGGACAGC-3'	This paper	Roche UPL: #46
hA2M qPCR primer 2 5'-GCTGGAAGACCTTGGTTTTTAC-3'	This paper	Roche UPL: #46
hC3 qPCR primer 1 5'-CCAAACTCAGCATCAACACAC-3'	This paper	Roche UPL: #20
hC3 qPCR primer 2 5'-AGAGCTCCTGCTTCTTCGTG-3'	This paper	Roche UPL: #20
hFGA qPCR primer 1 5'-GGAAATTTTGAGAGGCGATTT-3'	This paper	Roche UPL: #30
hFGA qPCR primer 2 5'-CCTCTGACACTCGGTTGTAGG-3'	This paper	Roche UPL: #30
hFGG qPCR primer 1 5'-GAAGGACAGCAACACCACCT-3'	This paper	Roche UPL: #19
hFGG qPCR primer 2 5'-GTAAATCTCTTTTGAAACGGTCTTTTA-3'	This paper	Roche UPL: #19
hFN1 qPCR primer 1 5'-GGGAGAATAAGCTGTACCATCG-3'	This paper	Roche UPL: #25
hFN1 qPCR primer 2 5'-TCCATTACCAAGACACACACACT-3'	This paper	Roche UPL: #25
hHAMP qPCR primer 1 5'-GACCAGTGGCTCTGTTTTCC-3'	This paper	Roche UPL: #36
hHAMP qPCR primer 2 5'- TCTGGAACATGGGCATCC-3'	This paper	Roche UPL: #36
hHP qPCR primer 1 5'-TGGAGTGTA CACCTTAAACAATGAG-3'	This paper	Roche UPL: #86
hHP qPCR primer 2 5'-TTCTTGGGC TTCCCACATAC-3'	This paper	Roche UPL: #86
hHPX qPCR primer 1 5'-TCACCGTG GAGAATGTCAAG-3'	This paper	Roche UPL: #35
hHPX qPCR primer 2 5'-CTCCTTCA TGGTTCCCGTAG-3'	This paper	Roche UPL: #35
hSERPINA1 qPCR primer 1 5'-CCATCT TCTTCCTGCCTGAT-3'	This paper	Roche UPL: #9
hSERPINA1 qPCR primer 2 5'-GGTAAA TGTAAGCTGGCAGACC-3'	This paper	Roche UPL: #9
hSERPINA3 qPCR primer 1 5'-ACTCCA GACAGACGGCTTTG-3'	This paper	Roche UPL: #42
hSERPINA3 qPCR primer 2 5'-ATTCTCT CCATTCTCAACTCTGC-3'	This paper	Roche UPL: #42
hSMAD6 qPCR primer 1 5'-GGGCAAAC CCATAGAGACAC-3'	This paper	Roche UPL: #10
hSMAD6 qPCR primer 2 5'-CGAGGA GACAGCCGAGAGT-3'	This paper	Roche UPL: #10
hID3 qPCR primer 1 5'-CATCTCCA ACGACAAAAGGAG-3'	This paper	Roche UPL: #59

(*Continued on next page*)

Continued

REAGENT or RESOURCE	SOURCE	IDENTIFIER
hID3 qPCR primer 2 5'-CTTCCGGCAGGAGAGGTT-3'	This paper	Roche UPL: #59
hCRP qPCR primer 1 5'-GAATTCAGGCCCTTGTATCACT-3'	This paper	Roche UPL: #18
hCRP qPCR primer 2 5'-ACACAAAAGCCTTCCTCGAC-3'	This paper	Roche UPL: #18
hHPRT qPCR primer 1 5'-TGACCTTGATTTATTTTGCATACC-3'	This paper	Roche UPL: #73
hHPRT qPCR primer 2 5'-CGAGCAAGACGTTCAGTCCT-3'	This paper	Roche UPL: #73
hGAPDH qPCR primer 1 5'-AGCCACATCGCTCAGACAC-3'	This paper	Roche UPL: #60
hGAPDH qPCR primer 2 5'-GCCCAATACGACCAAATCC-3'	This paper	Roche UPL: #60
hTBP qPCR primer 1 5'-CGGCTGTTTAACTTCGCTTC-3'	This paper	Roche UPL: #3
hTBP qPCR primer 2 5'-CACACGCCAAGAAACAGTGA-3'	This paper	Roche UPL: #3
hGUSB qPCR primer 1 5'-CGCCCTGCCTATCTGTATTC-3'	This paper	Roche UPL: #57
hGUSB qPCR primer 2 5'-TCCCCACAGGGAGTGTGTAG-3'	This paper	Roche UPL: #57
Software and algorithms		
Spectronaut	Biognosys	https://biognosys.com/software/spectronaut/
Limma	Ritchie et al.[47]	http://www.bioconductor.org/packages/release/bioc/html/limma.html
MSPypeline	Heming et al.[48]	https://github.com/siheming/mspypeline
BlotIt	Kemmer et al.[49]	https://github.com/JetiLab/blotIt
Mathematical model of HepG2	This paper	https://www.ebi.ac.uk/biomodels/MODEL2503270001
Mathematical model of PHH	This paper	https://www.ebi.ac.uk/biomodels/MODEL2503270002
Code described in this manuscript	This paper	https://zenodo.org/records/16411069

EXPERIMENTAL MODEL AND SUBJECT DETAILS

Isolation of primary human hepatocytes

Informed consent of the patients was obtained according to the ethical guidelines of University Clinics Heidelberg and Leipzig (registration number 322/17-ek, date 2020/06/10, ratified on 2021/11/30, registration number 422/21-ek, date 2021/11/10 and 178/16-lk, date 2016/07/12). PHHs isolation was performed in a standardized way as described earlier.[50] Non-cancerous PHHs were isolated from tumor-free liver tissue resected from human livers of the patients in Table 1.

For standard time-course and dose response experiments, 2×10^6 cells were seeded in 6 cm collagen I-coated tissue culture plates or 1.5×10^6 cells were seeded in 6 well collagen I-coated tissue culture plates (both BD Biosciences) in 2 ml or 1 ml of adhesion medium [phenol red-free Williams E medium (Biochrom) containing 10% (v/v) fetal bovine serum (Life Technologies), 0.1 μM dexamethasone, 10 μg/mL insulin, 2 mM L-glutamine and 1% (v/v) penicillin/streptomycin (Life Technologies)]. Cells were maintained at 37°C, 5% CO_2, and 95% relative humidity. After 4 h of adhesion, unattached hepatocytes were removed by washing 3 times with DPBS (PAN Biotech) followed by overnight cultivation in pre-starvation medium [phenol red-free Williams E medium containing 0.1 μM dexamethasone, 2 mM L-glutamine, and 1% (v/v) penicillin/streptomycin]. On the next day, cells were washed 3 times with DPBS and cultured for 6 h in starvation medium [phenol red-free Williams E medium supplemented with 2 mM L-glutamine, 1% (v/v) penicillin/streptomycin] prior drug, inhibitor or IL-6 treatment.

Cell culture

HepG2 cells were cultivated in a humidified cell culture incubator at 37°C and 5% CO2 and grown in growth medium [phenolred-free Dulbecco's modified Eagle medium (DMEM), 1% (v/v) L-Glutamine, 1% (v/v) Sodium Pyruvate, 1% (v/v) Penicillin/Streptomycin,

10% (v/v) Fetal Bovine Serum (all Gibco, Life Technologies)]. Cells were repeatedly tested for mycoplasma and only cells that were negative have been used for experiments. 1×10^6 HepG2 cells/well were seeded in 2 ml growth medium in cell-culture grade 6-well plates (Techno Plastic Products). After 24 h adhesion time, cells were washed twice with DPBS (Pan Biotech) and 1 ml starvation medium [DMEM, 1% (v/v) L-Glutamine, 1% (v/v) Penicillin/Streptomycin, 1 mg/ml BSA] was applied. After overnight starvation, cell treatment was carried out without medium replacement.

Drug, inhibitor and cytokine treatments

Recombinant human IL-6 was reconstituted in sterile filtered 0.3% BSA in DPBS. Recombinant human BMP-2 was reconstituted in sterile filtered 20 mM acetic acid. Diclofenac and acetaminophen were solved in DMSO. Actinomycin D was purchased from BioChemica (#A1489), dorsomorphin and LDN-193189 were reconstituted in DMSO. Maximum amount of DMSO applied on HepG2 cells was 0.5% and on PHH 0.25%.

Cell lysis and protein amount determination

For the whole proteome analysis of HepG2 cells 1×10^6 cells were seeded and treated as described above. For PHH 1.5×10^6 cells were seeded in 6 well collagen I-coated tissue culture plates (both BD Biosciences) as described above. After stimulation with different cytokine-drug combinations media was aspirated and cells immediately collected in ice-cold lysis buffer containing 25 mM Tris pH 7.6, 150 mM NaCl, 0.1 % SDS, 1 % NP40, 1 % Deoxycholic acid NA-salt, 1 mM Na_3VO_4, 10 mM NaF, 1 μg/mL Aprotinin, 0.1 mg/mL 4-(2-Aminoethyl) benzene sulfonyl fluoride-hydrochloride, 250 U/mL Benzonase, 10 U/mL DNase and PhosSTOP (4906845001 Roche: 1× Tablet/10 ml buffer) with a cell scraper. Benzonase, 10 U/mL DNase and PhosSTOP (4906845001 Roche: 1× Tablet/10 ml buffer). The total cell lysates were then incubated and rotated for 30 min at 4° C. Samples were centrifuged for 15 min at 14000 rpm and 4° C, and the supernatants were transferred to new vials. The BCA Assay (Pierce) was used to estimate protein concentration, and 5 μg of total protein was used per sample for further processing.

Preparation of cell lysate samples for mass spectrometry analysis

Protein digestion and clean-up were performed using an adapted version of the automated paramagnetic bead-based single-pot, solid-phase-enhanced sample-preparation (Auto-SP3) protocol[51] on a Bravo liquid handling platform (Agilent). Initially, protein disulfide bonds were reduced with 10 mM TCEP and alkylated with 40 mM CAA for 5 min at 95 °C. For bead preparation, Sera-Mag Speed Beads A and B (Cytiva) were vortexed until the pellet was dissolved. The suspension was placed on a magnetic rack, and the supernatant was removed after one minute. The beads were taken off the magnetic rack and suspended in water. This procedure was repeated three times. A total of 10 μL of bead A was combined with 10 μL of bead B, and the final volume was corrected to 100 μL with Ms-H2O. A total of 5 μL of A+B beads mixture was added to each sample. The Bravo liquid handling platform (Agilent) was operated using the "Auto-SP3" protocol provided by Agilent. 100mM TEAB buffer containing trypsin (enzyme/protein ratio of 1:25) was used for protein digestion, and samples were incubated overnight at 37 °C. After digestion, the recovered peptides were dried by vacuum centrifugation (1300 rpm at 45 °C), and stored at -80 °C until use.

Cell lysis for quantitative immunoblotting

For the preparation of total cell lysate for immunoblotting, cells were lysed in RIPA lysis buffer [2% (v/v) Nonidet P-40 (NP40, Roche Applied Sciences), 50 mM Tris pH 7.2, 250 mM NaCl, 2.5 mM EDTA, 0.5% (w/v) sodium deoxycholate (Serva), 200 μg/ml 4-(2-aminoethyl) benzenesulfonylfluorid (AEBSF), 2 μg/ml aprotinin, 1 mM Na_3VO_4, 10 mM NaF] after indicated treatment times. Samples were sonicated on ice (30 s, 75% amplitude, 0.1 s on, 0.5 s off). Subsequently, samples were centrifuged for 10 min at 14.000 rpm at 4°C and supernatants transferred into fresh test tubes.

For nuclear cytoplasmic fractionations, cells were lysed with cytoplasmic lysis buffer [0.4% (v/v) NP40, 10 mM HEPES, 10 mM KCl, 0.1 mM EDTA, 0.1 mM EGTA, 1 mM DTT, 1 mM NaF, 1 mM Na3VO4, 2 μg/ml aprotinin and 200 μg/ml AEBSF] and were centrifuged at 18.000 g at 4°C for 1 min. Supernatants were collected as cytoplasmic fractions. Nuclear pellets were washed with cytoplasmic lysis buffer without NP-40 and were incubated in nuclear lysis buffer [20 mM HEPES, 25% Glycerol, 400 mM NaCl, 1 mM EDTA, 1 mM EGTA, 1 mM DTT, 1 mM NaF, 1 mM Na3VO4, 2 μg/ml aprotinin and 200 μg/ml AEBSF), while constant shaking at 4°C for 15 min. After centrifugation at 18.000 g at 4°C for 15 minutes supernatants were collected as nuclear fractions.

METHOD DETAILS

Quantitative immunoblotting

Protein concentrations of lysates were quantified by BCA assay (Pierce, Thermo Scientific). For immunoprecipitation (IP) of target proteins, 500 μg of total protein lysates were incubated with respective IP antibodies and protein-A (for antibodies originating from rabbit) or protein-G sepharose (for antibodies originating from mouse) (both GE Healthcare) and were rotated at 4°C overnight. Precipitated proteins or 30 μg of total cell lysate, cytoplasmic or nuclear fractions were resolved by 10% SDS-polyacrylamide gel electrophoresis and transferred to 0.45 μm PVDF membranes (Immobilon P, Merck Millipore, #IPVH0010) according to established recommendations for quantitative immunoblotting.[52] Membranes were incubated with primary antibodies at 4°C overnight. Horseradish peroxidase (HRP) coupled secondary antibodies were applied at RT for 1 h. Antibody signals were either removed by β-mercaptoethanol/SDS-treatment prior to re-probing for a different protein or by inactivation of HRP by 15 min treatment with 30% H_2O_2

at 37° C. Phosphorylated species were detected first, followed by total proteins and housekeeping proteins. Proteins were visualized using enhanced chemiluminescence substrate (GE Healthcare) and signals were detected using a CCD camera (ImageQuant LAS4000, GE Healthcare). For band quantification, the ImageQuantTL (GE Healthcare) software was used.

Quantification of target gene expression by quantitative real-time PCR (qRT-PCR)

Cells were collected in RA1 lysis buffer (provided in the kit NucleoSpin RNA isolation, Macherey-Nagel) supplemented with 1% of β-mercaptoethanol and RNA was extracted using the NucleoSpin RNA isolation kit (Macherey-Nagel) according to the manufacturer's instructions. Reverse transcription of 1 μg of RNA was performed using the High Capacity cDNA Reverse Transcription Kit (Applied Biosystems). The following conditions were employed: Step 1: 25°C, 10 min; step 2: 37°C, 120 min; step 3: 85°C, 10 min, step 4: 4°C until sample was removed. Diluted cDNA (1:11) was analyzed applying the Universal ProbeLibrary System on a LightCycler 480 (both Roche) with the PrimaQuant qPCR Probes Master (Steinbrenner). The following cycling conditions were employed: Pre-incubation: 95°C, 2 min, 4.4°C/s ramp rate. 50 cycles with melting: 95°C, 10 s, 4.4°C/s ramp rate; primer annealing: 60°C, 30 s, 2.2°C/s ramp rate; DNA synthesis: 72°C, single acquisition, 1 s, 4.4°C/s ramp rate. Cooling: 40°C, 2 min, 1.5°C/s ramp rate. Relative mRNA concentrations were calculated according to a cDNA dilution series with the Absolute Quantification Second Derivative Maximum method of the LightCycler 480 Basic Software (Roche). Target mRNA concentrations were normalized to the geometric mean of housekeeper concentrations. Primer/probe combinations were designed using the Universal ProbeLibrary Assay Design Center (Roche).

Bead-based immunoassay and ELISA

Cells were seeded, growth factor deprived and stimulated as described before for the corresponding cell type. At the start of each experiment and after the indicated treatment time, cell culture medium was collected and centrifuged to pellet cell debris at 1.000 g and 4°C for 10 min. The supernatant was transferred into a fresh reaction tube and stored at -80 °C. Human BMP-4 in the cell supernatant was analyzed with the help of a magnetic Luminex Assay (R&D Systems) according to the manufacturer's recommendation, using a BioPlex 200 System (BioRad). Human BMP-2 in the cell culture supernatant was analyzed using a Human BMP-2 Quantikine ELISA (R&D Systems), which was read at a F200pro plate reader (Tecan).

Global Mass Spectrometry (MS)

All samples were analyzed with an Ultimate 3000 HPLC (Thermo Fisher Scientific) coupled to an Orbitrap Exploris 480 mass spectrometer (Thermo Fisher Scientific). Tryptic peptides were dissolved in 15 μl loading buffer (0.1 % formic acid (FA), 2 % ACN in MS-compatible H_2O), and 2 μL were injected for each analysis. The samples were loaded onto a pre-column (PEPMAP 100 C18 5 μm 0.3 mm × 5 mm, Thermo Scientific) using a loading pump at a higher flow rate. After 4 min, a valve was switched, and peptides were delivered to an analytical column (75 μm × 30 cm, packed in-house with Reprosil-Pur 120 C18-AQ, 1.9 μm resin, Dr. Maisch) at a flow rate of 5 μL/min in 98 % buffer A (0.1 % FA in MS-compatible H_2O). After loading, peptides were separated using a 141 min gradient from 8% to 38% of buffer B (0.1% FA, 80% ACN in MS-compatible H_2O) at a 300 nL/min flow rate. The Orbitrap Exploris 480 mass spectrometer was operated in data-independent mode (DIA), with an m/z range of 350-1400. Full scan spectra were acquired in the Orbitrap at 120 000 resolution after accumulation to the set target value of 300 % (100 % = 1e6) and maximum injection time of 45 ms. DIA scans followed the full scans. Forty-seven isolation windows were defined, with an m/z range of 406-986. Spectra were generated in the orbitrap (isolation window 1 m/z) after fragmentation using higher energy collisional dissociation (HCD) at normalized collision energy (N)CE of 28 % and acquired at 30000 resolution after accumulation to the set target value of 1000 % (100 % =1e5) and maximum injection time of 54 ms.

Database search and data analysis

All DIA raw data files were analyzed with a direct DIA workflow using Spectronaut (version 18.7, Biognosys) with the built-in Pulsar search engine. The Uniprot Homo sapiens reference proteome database (#UP000005640, downloaded on 21st February 2023) was used for the Pulsar search. The default settings for database match include full specificity trypsin digestion, peptide length of between 7 and 52 amino acids, and maximum missed cleavage of 2. N-terminal methionine was removed during preprocessing of the protein database. Carbamidomethylation at cysteine was used as a fixed modification, and protein N-terminal acetylation and methionine oxidation were set as variable modifications. The false discovery rates (FDRs) were set as 0.01 for the peptide-spectrum match (PSM), peptide, and protein identification. For quantification, identified (Qvalue) was set for precursor filtering and MS2 quantification with the area as quantity type. The original mass spectrometric raw files Spectronaut files are available on the proteomeXchange PRIDE platform.[45]

QUANTIFICATION AND STATISTICAL ANALYSIS

Statistical analysis of DIA data

For the biological interpretation of the proteomics data, the protein table output was preprocessed using MSPypeline, a python-based proteomics pipeline.[48]

Mathematical modeling

Mathematical multi-compartment models were developed and described by sets of coupled ordinary differential equations (ODEs) implemented using the Data2Dynamics software package.[53] We employed the linear chain trick method to model time delays e.g. for SOCS3 mRNA synthesis.[54] The linear chain trick models the delay function as a series of intermediate steps reflecting biological processes more appropriately. In each simulated experiment, the model was equilibrated to steady-state prior to *in silico* treatment with inhibitors or stimulation. All model parameters were estimated directly from the experimental data using Maximum Likelihood Estimation. Several experiments required the use of scaling, offset and error model parameters that were estimated simultaneously with the dynamic parameters. To assess parameter identifiability, profile likelihood calculation was performed after each iteration.[28] This was then followed by either model reduction[55] or additional data acquisition. For a full mathematical description of the mathematical models, including profiles and time courses, see supplemental methods.

Plotting

Model time-courses were typically fitted with scaling and/or offset parameters in the observation function. To facilitate showing all the data for a particular observable in a single plot, the observation function was inverted. Data point means were computed from the inverted means, while error bars were calculated by means of averaging the estimated error variances determined by the observational error model. Model trajectories and data were plotted in the space where fitted (linear for immunoblotting data and logarithmic for gene expression data).

L_1-regularization

To identify potential candidate drug targets, an L_1-regularization approach was applied.[56] In this approach, every model parameter was modulated by an additionally estimated parameter Δ_k, that mediated the effect of the drug on the respective reaction following the formula:

$$k' = k(1 + \Delta_k[drug](t))$$

To enforce a sparse solution, estimated changes induced by the drug were penalized using an L_1 prior. This gave rise to the following -2 log likelihood function to be minimized:

$$-p\log(L) = \sum_{i=1}^{N_{obs}}\left(\left(\frac{y_i - g(x,p))}{\sigma_i(x,p)}\right)^2 + 2\log(\sigma_i(x,p))\right) + \lambda\sum_{k=1}^{N_\Delta}|\Delta_\kappa|$$

Here y_i referred to the data, $g(x,p)$ was the model depending on the states x and the parameters p. The standard deviation of each data point was provided by the error model and denoted by $\sigma_i(x,p)$. The regularization strength was denoted by λ. This prior penalized the absolute difference from zero for our drug effect parameters. To study the effect of regularization, we performed parameter optimization over a large range of regularization strengths λ. Consequently, when sorted by the regularization strength, parameter changes were sequentially pushed to zero at the cost of fidelity to the data. Estimating model parameters was challenging, and the possibility existed that for any given regularization level, there might be multiple local optima. To mitigate the risk that we missed the most optimal parameterization we repeated the optimization procedure 1000 (if not indicated otherwise) times for every regularization level, starting from widely dispersed initial values.

After optimization, parameter changes, which were pushed to zero were fixed to zero (reduced from the model) and the penalty of other parameter changes was removed. This was then followed by re-optimization to avoid biasing the parameter estimates of the inferred effects. During our early analyses, we found that the model would sometimes use regularization parameters to improve the fit of the control situation. Since this hampered analysis, we decided to keep the control parameters fixed while performing the L_1-regularization. After completion of the large regularization scan, fit quality was assessed using the Bayesian Information Criterion (BIC):

$$BIC = \log(n)\kappa - 2\log(L)$$

Here, n refers to the number of data points, κ is the number of free parameters in the model and L represents the likelihood. Accordingly, a lower BIC value indicates a better fit. Note that as the number of parameters κ increased, the BIC increased as well hereby penalizing model complexity.